Estimates of the signal band of the Blackfoot broad-band data

Gary F. Margrave

ABSTRACT

A unique seismic dataset was acquired over the Blackfoot field (owned by PanCanadian Petroleum Ltd) in the summer of 1995. The acquisition was designed to collect a dataset which would allow a thorough analysis of the factors controlling the bandwidth of seismic data and, hopefully, would lead to new strategies for extending that bandwidth. The dynamite source was recorded simultaneously into four distinct receiver configurations: conventional 6 phone (10 Hz) vertical component strings, single 10 Hz 3 component phones, single 4.5 Hz 3 component phones, and 2 Hz 2 component phones. This work presents a spectral analysis of the data, both raw and processed, to compare the performance of the different receivers, to identify the derived signal band of the processed data and to estimate the potential signal band on the raw data. It is found that the different receiver types performed in a broadly similar fashion though the low frequency models recorded markedly more power at the low end. No high end signal distortion was observed on any model. The signal band of the processed vertical components, as defined by f-x phase coherence, tops out near 100 Hz in the shallow section and decays to 75 Hz of so near basement. Corner frequencies estimated from the raw data give similar results indicating that the data processing has fully extracted the available signal. On the radial components, the processed data tops out in the 30-40 Hz range while the raw data show corner frequencies near 65 Hz. Either the data processing has failed to image the upper P-SV frequencies or P-P energy has leaked onto the radial components. On the low end, all processed data show f-x phase coherence to well less than 5 Hz. It is anticipated that this represents extended signal band and that impedance inversions should benefit from it.

INTRODUCTION

The Blackfoot broad-band experiment was conducted in the summer of 1995 over the Blackfoot field (southeast of Strathmore, Alberta, and owned by PanCanadian Petroleum Ltd.). A major purpose of the experiment was to record a high source effort wavefield simultaneously into a variety of different receivers with the intent to compare their performance. The acquisition of the survey and the current status of the interpretation are described elsewhere in this years CREWES report so only those details relevant to the signal analysis will be discussed. The line was 4km in length, trending northwest to southeast, and had 200 receiver positions at 20m spacings. Source effort was a 6kg dynamite charge at 18m depth with a shot between each pair of receiver stations. The entire line was live for each shot resulting in end-on geometries with 4km maximum offsets at the ends of the line grading to split-spreads in the center with 2km far offsets. Stacking fold exceeded 100 near the middle of the line. Station 101 was at the southeast end of the line and station 300 was at the northeast end. Recording length was 6 seconds and the data were sampled at 1 ms. Four types of receivers were used:

- 10 Hz array: This was intended to represent standard industry practice and consisted of single component (vertical) phones in a six phone string. The receiver array was spread out over one receiver interval (20 m) and so had only a minor

directivity effect. These were Oyo GS-30ct with a spurious resonance supposedly near 100 Hz.

• 10 Hz 3-C phones: A single 10 Hz 3-C phone was deployed at each receiver location. These are Litton model LRS-1033 phones and may be the most common 3-C phone in use today.

• 4.5 Hz 3-C phones: Single 4.5 Hz 3-C phones were also deployed at each receiver station. While not as common at the 10 Hz 3-C phones, they are still readily available commercially from Mark Products as their L-28 and may have a spurious resonance at 90 Hz. These were scheduled to be used by Lithoprobe in Alberta just after the Blackfoot survey and we are grateful to Iris/Passcal (Stanford, California) and the Lithoprobe project for making them available.

• 2 Hz vertical and horizontal phones: These phones were single component low frequency phones which were also available to us because they were being brought to the province by Lithoprobe for deep crustal recording. Also made by Mark Products as their L-4, they have a reported spurious resonance at 40 Hz. Unlike the other phones, they mount in cradles rather than with spikes and had to be very carefully laid out. A vertical 2 Hz phone was deployed at each receiver location while horizontal phones were deployed in radial (inline) orientation at receiver locations 153 through 213.

With the exception of the first 30 or so stations on the southeast, most of the line was pasture with a loose surface till. The southeast end trended slightly uphill and, as will be seen, had markedly different near surface properties. The 10 Hz array was simply planted at surface, the 10 Hz 3-C and 4 Hz 3-C phones were planted in 20 cm holes but not buried, and the 2 Hz phones were completely buried at 30 cm. The multicomponent phones were carefully leveled and oriented.

The data has been processed by Sensor Geophysical Ltd. and Pulsonic Geophysical Ltd. and is currently being processed within the CREWES group. All the processed data examined in this report all was produced by Sensor. No attempt will be made to compare the quality of the different processing. The Sensor data was used simply because it was readily available.

The use of receivers with a low resonance frequency was motivated by a desire to extend the typical seismic bandwidth on the low end. Commonly, seismic data is filtered to reject frequencies below 10-12 Hz on the *assumption* that they contain no usable signal. Certainly surface waves of various types flood the low frequency band; but, with 24 bit modern recording systems there should be sufficient dynamic range to recover reflection signals in these frequencies (if they exist). Such low frequency reflection energy would be of great benefit in seismic resolution and especially inversion for impedance (Hendrick and Hearn 1993, Oldenburg et al. 1983). Thus a major goal was to see if this could be done without any sacrifice of high frequency signal.

SIGNAL BAND ESTIMATION METHOD

There are a great variety of methods which have been proposed to estimate the signal band of seismic data. Perhaps the most commonly used discriminator between signal and noise is "alignment". Most often, the goal of pre stack processing is the time alignment of signal on cmp (common midpoint) or ccp (common conversion point)

gathers so that they stack coherently. Gain and deconvolution attempt to equalize signal in amplitude and bandwidth which assists the later processes of residual statics and velocity analysis which are directly aimed at data alignment. Thus, one perspective on the pre stack processing flow is that it is a sophisticated signal band detection system which has the collective wisdom and experience of an entire industry behind it.

The approach taken here is to examine the spectral character of the final stacks through the use of interpretive visual displays. This is in contrast to approaches which use a mathematical estimator (such as semblance) (Yilmaz 1987) which usually fail to convey a clear, detailed picture of the signal band. Also, the very notion of "signal band" is complex and suggests a somewhat unrealistic concept of seismic data. For impulsive sources, signal is not confined to any particular frequency band; but instead, tends to mix with coherent and random noise in a complex pattern. Statements of the upper and lower frequencies forming the "signal band" must always be taken as best guesses and treated as a moving target. There is no specific frequency at which signal ends and noise begins; rather, there is a continuous transition from "signal dominated" frequencies to "noise dominated" with no clear boundary.

Additionally, the nature of the data processing must also be considered. Estimates made directly on raw data are often overly pessimistic because they lack the tremendous benefit of the pre stack processing sequence. (However a method will be examined here which agrees closely with results from the final stack analysis.) Estimates made on migrated sections are also problematic because multichannel processing causes high inter-trace correlations throughout the frequency band. A final stack is thus an optimal product on which to conduct signal band analysis.

One of the most successful signal enhancement techniques is f-x prediction filtering (also called f-x deconvolution) and is usually run on stacked data. This method succeeds because signal shows "phase coherence" while noise does not. Phase coherence simply means that the phase of the seismic data, considered as a dataset in the f-x domain, is consistent (predictable) at constant f and trending x. Thus the analysis will consist simply of transforming and displaying the data in f-x space in a suitable fashion. The method used here was developed by me while I was employed by Chevron and has been used for about six years. I have recently received permission to publish the technical details and will do so in the very near future. In this paper, I will simply display the results which are quite interpretable without the algorithm details.

ANALYSIS OF THE FINAL STACKS

Figures 1 through 6 show the final stacks (Sensor processing) for the four possible vertical components (10 Hz array, 10 Hz vertical component, 4.5 Hz vertical component, and 2 Hz vertical component) and the 10 and 4.5 Hz radial components (the 2 Hz radial stack was not available). In all cases the displays are limited to roughly "above basement" which means down to 1.6 seconds for P-P data (vertical components) and 2.6 seconds for P-SV data (radial components). The pre stack processing flow included f-k filters on shot records, surface consistent spiking deconvolution, TVSW (time variant spectral whitening), refraction and residual statics, and velocity analysis. For vertical components, the TVSW band was 0/1-100/120 Hz with a 500 ms operator while for the radial components it was 0/1-70/80 Hz and a 750 ms operator. Post stack processing was only trace equalization over a single time window. The final filters selected (by the data processor) for migration can be considered as an estimate of signal band. For the vertical components, the trapezoidal

filter frequencies were 8-12-75-85 Hz while for the radial components they were 6-10-30-36. (These filters are NOT applied to the stacks shown and analyzed here.)

As can be seen, the vertical component stacks are all very similar to one another and so too the radial components. This immediate impression that all receivers performed very similarly is partially supported by the forthcoming analysis; however, we will also find significant differences. Also it is stressed that the processing was designed to optimally detect and whiten the signal band of each dataset and so tends to remove the receiver response function. Indeed, a number of the processing steps, especially TVSW, are very powerful "equalizers". The analysis of the raw spectra will show notable differences between the receiver types.

Single gated F-X spectra.

Figures 7 through 12 show f-x spectral displays for the corresponding stacked sections. As these are all essentially similar, consider figure 8, the f-x spectra over the time zone .1 to 1.6 seconds for the vertical component of the 10 Hz 3-C phones. The upper half of the figure is the f-x amplitude spectrum plotted as a single wiggle trace for each time domain trace. The spectra are displayed as linear (i.e. not in decibels) and black indicates high power. The lower half of the figure is an f-x phase display, again plotted as a single wiggle trace for each time domain trace. Though these are 2 ms data with a Nyquist frequency of 250 Hz, only the first 120 Hz are displayed. Several key elements of interpretation are:

- Spectral continuity in either display indicates signal. Conversely, noise is chaotic, especially in the phase display.

- The time domain display is formed mainly by those frequencies appearing as dark black in the amplitude display. When plotted as linear spectra with the maximum amplitude just clipped, the dynamic range of the amplitude display is about 12-15 db which is the same as a time domain wiggle plot.

- Ideally processed data will have high spectral power where the f-x phase shows coherence and low power where it is chaotic.

- These spectra must be considered as representing average properties over the time zone from which they are derived.

One of the first things to notice is that the high frequency signal limit varies quite strongly across the section. Over stations 101 to about 130, we see phase coherence at least to 90 Hz and hints of it still higher. As we progress towards station 300, the signal band gradually drops below 80 Hz. So we can see some justification for the final filter specifications as tuned for the "lowest high frequency" along the line. The higher bandwidth around the beginning of the line correlates with the elevated topography there and is probably indicative of a less absorptive near surface.

The three stacks of vertical components form 3-C receivers show very similar high frequency limits which is a bit surprising especially in the 2 Hz case. The 10 Hz array seems stand out with patches of phase coherence at higher frequencies than the others, for example, near station 150. These patches seem to be of a different character than elsewhere on the section and it is not known if they represent reflection signal.

Also apparent is the "hole" in the signal band trending from around 60 Hz at station 160 to 50 Hz at station 260. This is characterized by low power on the amplitude

display and poor coherence on the phase display. A likely explanation for this is a surface ghost (figure 13). It is well known that a ghost puts a notch in a spectrum at a frequency of $f=1/\Delta t$ where Δt is the two way time from a buried source to the surface. With an effective source depth of about 15 meters, a weathering velocity of 1700m/s puts the notch at 57 Hz. Perhaps the beginning of the line had a much faster weathering velocity which moved the notch to higher frequencies.

On the low end, we see encouraging hints of phase coherence at very low frequencies. All receivers show coherence down to 5 Hz and is seems that the 4.5 and 2 Hz sections go lower than that. An inversion experiment should be effective in determining the extent to which these coherent frequencies can be regarded as reflections. That is, a determination of the lowest seismic frequency which still improves the quality of an impedance inversion would be definitive.

The two radial component spectral displays (figures 11 and 12) are very similar to one another. Phase coherence seems to end abruptly at just over 40 Hz and to change character at 30 Hz. Also there is little evidence of a higher signal band near stations 101 to 130 as on the vertical component sections. A possible explanation is that the effect is entirely due to the surface ghost, which would be at the same frequency for P-SV and for P-P and thus entirely outside of the signal spectrum. On the low end, phase coherence drops dramatically at about 4 Hz but seems slightly better on the 4.5 Hz section.

The high degree of similarity between the various spectral sections might seem surprising. As already mentioned, the processing attempts to achieve this; but, given the very different technical specifications of the receivers, it seems to have succeeded beyond expectation. For example, the 2 Hz sections might have been expected to show some degradation on the high end but this seems very slight if present at all. Also, there is no evident anomaly anywhere near the anticipated spurious resonance at 40 Hz.

Time variant F-X spectra

Since the spectra of figures 7-12 must be considered as averages over the entire sedimentary section, the construction of similar displays over shorter time windows is immediately suggested. Figures 14-17 show time gated F-X analyses for the four vertical component stacks using gates of: .1 to .6 seconds, .6 to 1.1 seconds, and 1.1 to 1.6 seconds. Similar products for the radial components are shown in figures 18 and 19.

Consider the time variant analysis for the 10 Hz vertical components. The shallow time zone shows the broadest signal with a high end near 120 Hz though on the single vertical array there is markedly greater phase coherence above 100 Hz. In the middle time zone, the high end of the signal band has dropped to 80-90 Hz and decreases further to around 70-80 Hz in the lower time zone. In all cases, the 10 Hz array has achieved slightly better phase coherence at the high end. On the low end, there is apparent phase coherence at very low frequencies in all time zones.

Though the 10 Hz array seems to have a slight edge in phase coherence, the single components have performed very well. It is reasonable to expect that post stack f-x prediction filtering might equalize these sections to a very high degree. This is very encouraging since the field effort to lay out a 3-C array is high while a single 3-C phone can be planted in a time comparable to an array of vertical phones.

At the low end, all of the detests are largely similar and all have apparent phase coherence at very low (less than 5 Hz) frequencies. This is encouraging in light of the goal of recording low signal frequencies but more work needs to be done to verify that these are truly reflection signals.

The radial components show a similar picture with a signal high end exceeding 40 Hz in the shallow section and decreasing to around 30 Hz in the bottom zone. Both receiver types show phase coherence below 5 Hz.

Average amplitude spectra

Figures 20 and 21 show average amplitude spectra for the various receiver types and time windows discussed so far. The displays show the various spectra vertically displaced from one another so that they may be easily compared. Each spectrum is a simple numerical average of the f-x amplitude spectra already examine and is displayed in decibels relative to its own maximum. As these are averages across the entire stacked section they represent only gross behavior. Still, they are amazingly similar and fairly close examination is required to spot any differences. The overall spectral shape is almost entirely a function of the data processing with the TVSW process being the most influential. On figure 19, which compares the vertical components, we can see slightly more power in the 2 and 4.5 Hz data at the very lowest frequencies (consider the .1 to .6 second window) and slight differences in the 80 to 120 Hz range. As Figure 20 shows, the story is very much the same with the radial components.

ANALYSIS OF RAW DATA

The examination of the processed data yielded firm estimates of the derived signal band for each receiver type and the general impression that the receivers performed with approximate equivalence. As has been mentioned, these conclusions are strongly dependent on the data processing so an examination of the raw data will now be conducted. It is hoped that there will be features in the raw records which predict the eventual signal band and which will provide more information in the receiver comparison. After some deliberation, shot 101 was selected because that end of the line showed higher signal band after processing and because the end on geometry would show more offsets.

Figures 22-25 show the vertical components for shot 101 after the application of spherical divergence corrections only (the displays show the higher amplitudes clipped in order to bring out some reflection detail). The radial components are shown in figures 26-28. (Note that 2 Hz radial receivers were only available for stations 153 through 213.) It is immediately apparent that there are large differences in the receiver responses at this stage. Of first note is the increasing intensity of the discursive, low frequency surface waves as we move from the high to low frequency receivers. Since, to first order, all of these datasets yield similar signal bands after processing, it follows that current processing is quite capable of recovering reflection signal from beneath such surface waves.

F-X spectra of the shot records

The examination of f-x spectra on raw records is usually not as revealing as on stacked sections because the phase coherence of unaligned data is more difficult to see. Also, there are many non-reflection wave types on raw records which influence the phase coherence masking the reflection phase coherence. Nevertheless, there is much to

be learned so f-x spectra for each vertical receiver are shown in figures 29-32 while the radial receivers are in figures 33-35.

An illustrative example is provided in figure 30 which shows the f-x spectra for the 10 Hz vertical component. Spectra from two different time windows: 0 to 6 seconds (the entire record) and 0 to 2 seconds (the primary reflection zone). Some features of note are:

- The broad low frequency (under 10 Hz) arc of the surface waves.
- The dominant frequency band of 10-30 Hz which is mainly refractions (first breaks)
- Reflection energy, seen as spectral events curving down to the left. They are most easily seen on the amplitude spectra from stations 160 to 240.
- A great deal of phase coherence all through the record. Note especially the perpetuation of coherence practically to dc.
- The amplitude displays have limited dynamic range so the high energy surface waves dominate the lower frequency receiver displays.

Average amplitude spectra

The difficulty in analyzing the f-x spectra of the raw shot 101 is partly due to the great variety of wave types present. The analysis can proceed by examining average amplitude spectra over selected space-time gates which isolate waves of interest. Figure 36 shows the gates used for the analysis of the vertical components displayed on top of the 4.5 Hz record. The eight zones selected were chosen to isolate the major noise trains as well as several examples of reflections.

Figures 37-39 show the spectra from each of the four receiver types for each of the analysis zones. These spectra are displayed with a decibel scale where each spectral curve is in db down from its own maximum. For clarity, curves 2-4 in each plot have been displaced down by -10,-20, and -30 db respectively. Two plots are displayed for each zone: on the left is the entire spectrum out to 200 Hz while on the right is an enlargement of the first 80 Hz. Spectral averages over non uniform (changing size) gates are computed by normalizing each individual spectrum for its gate length and then averaging.

Spectra from zone 1 apply to the entire six second record length and are averages over the entire shot except for the inside ten offsets. (These inner offsets tended to be extremely affected by source noise and, among other things, contribute a large dc component.) The four receiver spectra are quite similar at high frequencies with small spectral peaks occurring reliably on all curves. Below 10 Hz, there is a marked increase in power on the low frequency phones. There is no evidence of any systematic distortion on any of the receivers for such things as "spurious resonance". The sharply defined band between 10 and 30 Hz is largely formed by the first breaks (see the results from zone 4).

The spectra from noise dominated gates (3,4 and perhaps 5) are included because they define the spectral shape of these noise types and facilitate their recognition when they leak into other analysis zones. So, zone 3 illustrates the sharp low frequency peak

of the dispersive surface waves while zone 4 shows the box shaped spectrum of the refractions.

Of greater importance are the spectra from the reflection dominated zones 6,7, & 8. In examining these, it is important to realize that simple constant Q theory (Kjartannson 1979) predicts an exponential decay of spectral strength with increasing frequency which, on these db displays, is indicated by a linear trend down to the right. Furthermore, a flat spectrum is one which shows no decay and is therefore not compatible with propagating wave in an attenuating medium. The spectra from zone 6 show the expected quasi-linear decay out to about 100 Hz. A "corner frequency" can be defined which is the intersection point between the decaying spectrum of propagating waves and the flat "background noise" spectrum at higher frequencies. This corner frequency is an estimate of the highest signal frequency and, in zone 6, is roughly around 100 Hz. In zones 7 and 8 we would pick around 70 to 80 Hz for the corner frequency. These estimates confirm those obtained from the final stack spectral analysis (see figures 14-17). The implication is that the data processing of the vertical component data has been very successful in imaging the potential signal bandwidth of the data.

On the low end, zones 6, 7, and 8 indicate significant spectral strength well below 5 Hz. The 2 and 4.5 Hz spectra show a much flatter spectrum over the 0-30 Hz range than do the 10 Hz phones. For the high end of the spectrum, it could be argued that propagating wavefields persisted to at least 100 Hz because their characteristic decay was observed. The same argument cannot be applied at the low end so, on the basis of average spectra alone, it cannot be proven that this low frequency power is reflection signal. However, phase coherence was observed on the processed data in this range so these are at least consistent results.

Figure 40 shows the spectral analysis zones defined for the radial components. Choice of zones was again to facilitate examination of the various noise trains as well as the reflection data. In zone 1, the spectra from the entire record are compared. As before, the inner ten offsets have been excluded from the spatial averaging. Also, the 2 Hz data was only averaged over stations 153-213 where it was collected. Again the spectra are broadly similar with the expected increase in power at low frequencies on the low frequency phones.

The spectra from zone 7 (and to some extent zone 5) are very interesting since these are expected to be reflection dominated. Using the same logic as for the vertical components, a corner frequency can be picked somewhere in the 60 to 70 Hz range. This is well in excess of the signal spectrum that was realized by data processing (see figures 18 and 19) where only about 30-40 Hz was coherently imaged. There are several possibilities to explain this discrepancy including:

- The corner frequency analysis may be invalid. This seems unlikely in view of the results with the vertical components and because it is an elementary prediction of attenuation theory.

- The data processing of radial component data for P-SV waves may be falling well short of its potential. Given the relative youth of this subject compared to vertical component processing, this may indeed by the case.

- The high frequencies observed in the average spectra between 40 and 70 Hz may correspond to P wave energy which has leaked onto the radial component. This also seems likely but it is difficult to argue it conclusively.

It seems likely that some combination of second and third possibilities will explain these observations. If the additional signal band can be shown to be propagating P-SV waves, then there is the promise of increasing the signal bandwidth of such data by about a factor of two. Alternately, if the additional signal band is dominated by P-P data leaking onto the radial component, then perhaps the P-SV bandwidth is already being fully recovered.

CONCLUSIONS

The Blackfoot dataset represents a very thorough scientific comparison of a variety of receiver types recording the identical physical wavefield. This work has only scratched the surface of what can be done with the dataset. Nevertheless, some conclusions seem apparent:

- The four different receiver types performed in a broadly similar fashion. A variety of minute spectral details were faithfully recorded by each. There is no indication of any sort of systematic distortion such as a spurious resonance.

- The vertical component processed data has a high end signal cutoff, indicated by f-x phase coherence, of about 100 Hz in the shallow section (less than .6 seconds) and decaying to 75 Hz near the Precambrian basement. All four receiver types were very similar here but the vertical array probably had a slight edge.

- Analysis of the vertical components on raw shot records shows a high end corner frequency that is in close agreement with the signal band observed on the processed data. It is deduced that the data processing has extracted virtually all of the available propagating wavefield signal.

- On the low end, the processed vertical components show phase coherence to well below the resonance frequency of each receiver type. The 2 and 4.5 Hz phones probably have a slight edge here but the even the 10 Hz receivers show coherence to 4 Hz and below.

- The radial component processed data has a high end signal cutoff around 40 Hz in the shallow section which decays to 30 Hz near basement. Both the 10 and 4.5 Hz receivers gave similar results. The 2 Hz radials were not analyzed as processed data.

- On the raw radial records, a corner frequency in the neighborhood of 65 Hz is visible. This conflicts with the measurements on the processed radial components. It is suggested that either there is a greater P-SV bandwidth than has so far been realized or that the additional band is P-P energy leaked onto the radial components.

ACKNOWLEDGMENTS

I am grateful to the sponsors of the CREWES project for funding the acquisition of the Blackfoot survey. I thank the members of the CREWES project who volunteered their time and effort during the field layout and pickup. The competent data processing of Sensor Geophysical is much appreciated. In particular, I thank Stan Gorek for his help in getting the various datasets ready for spectral analysis. Finally, I thank Chevron Corporation for allowing me to use and publish the f-x transform method of signal band analysis.

REFERENCES

Hendrick, N, and Hearn, S, 1993, Evaluation of Seismic Trace Inversion Techniques, Exploration Geophysics, 24, 549-560

Kjartannson, E, Constant Q - Wave propagation and attenuation, J. Geophys. Res., 84, 4737-4748

Oldenburg, D.W., Scheuer, T., and Levy, S., 1983, Recovery of the acoustic impedance from reflection seismograms, Geophysics, 48, 1318-1337

Yilmaz, O., 1987, Seismic Data Processing, Society of Exploration Geophysicists,

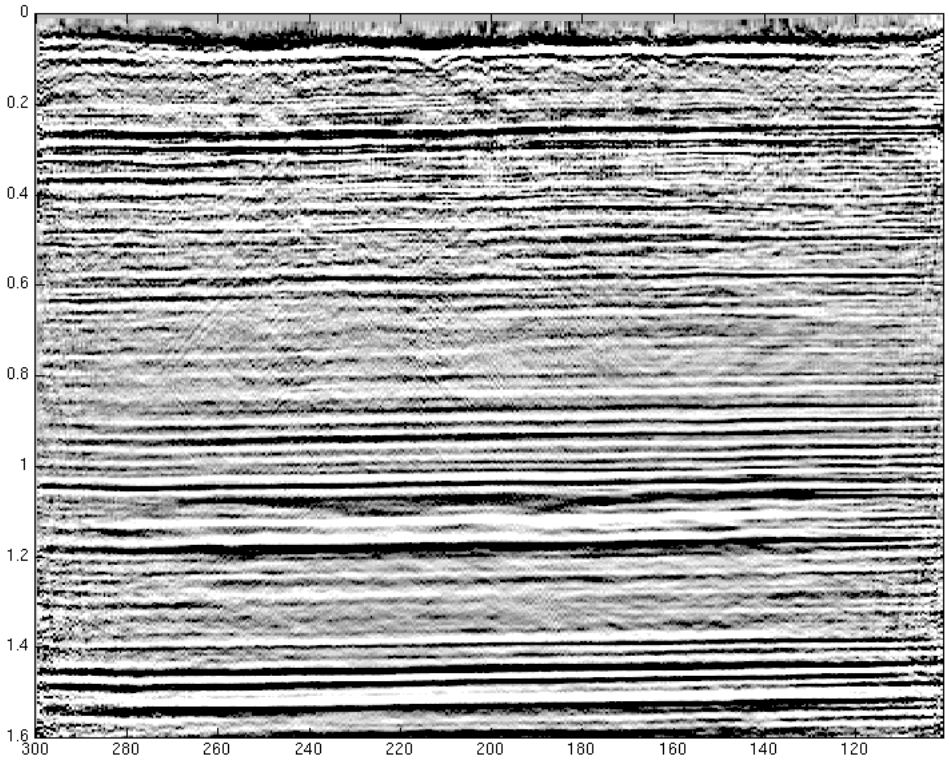

Fig. 1. Final stack for the 10 Hz vertical array data.

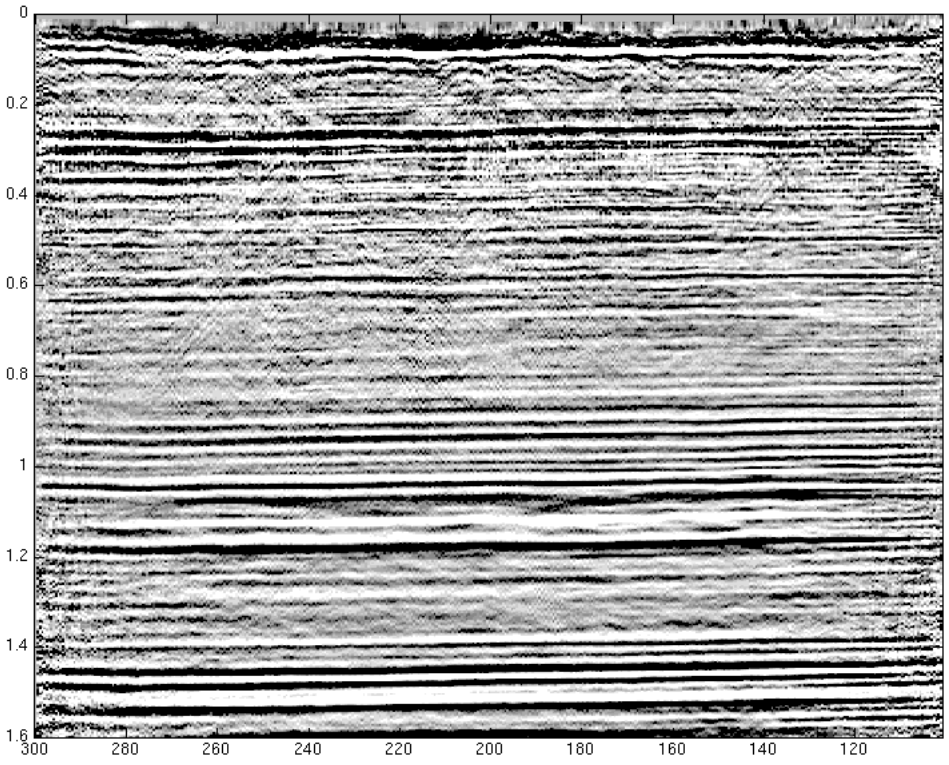

Fig. 2. Final stack 10 Hz vertical component.

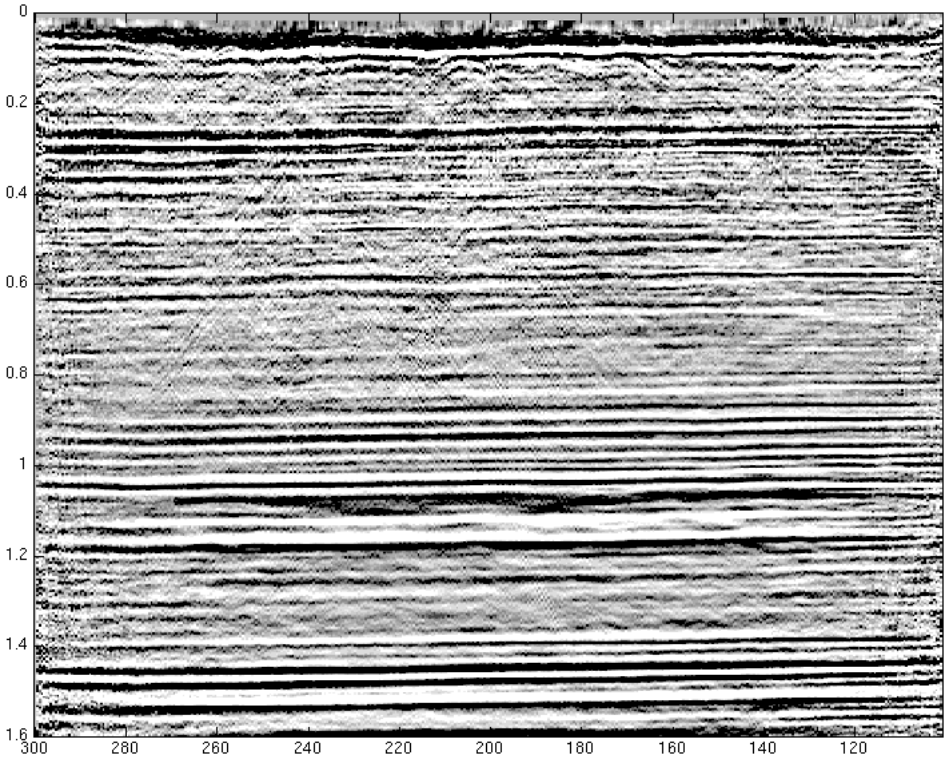

Fig. 3. Final stack 4.5 Hz vertical component.

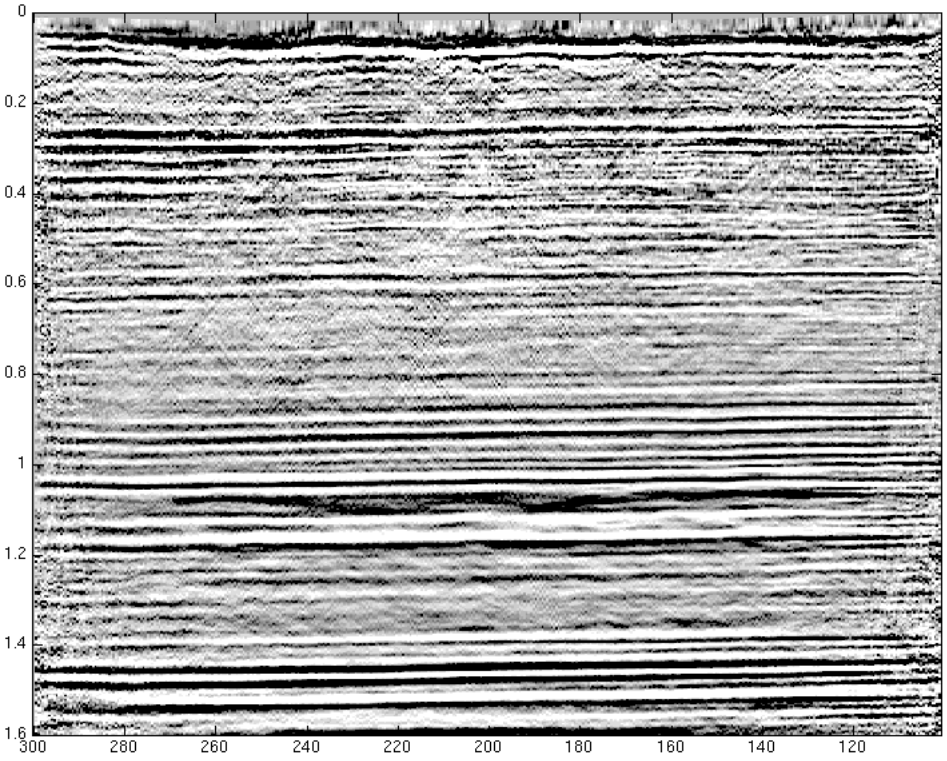

Fig. 4. Final stack 2 Hz vertical component.

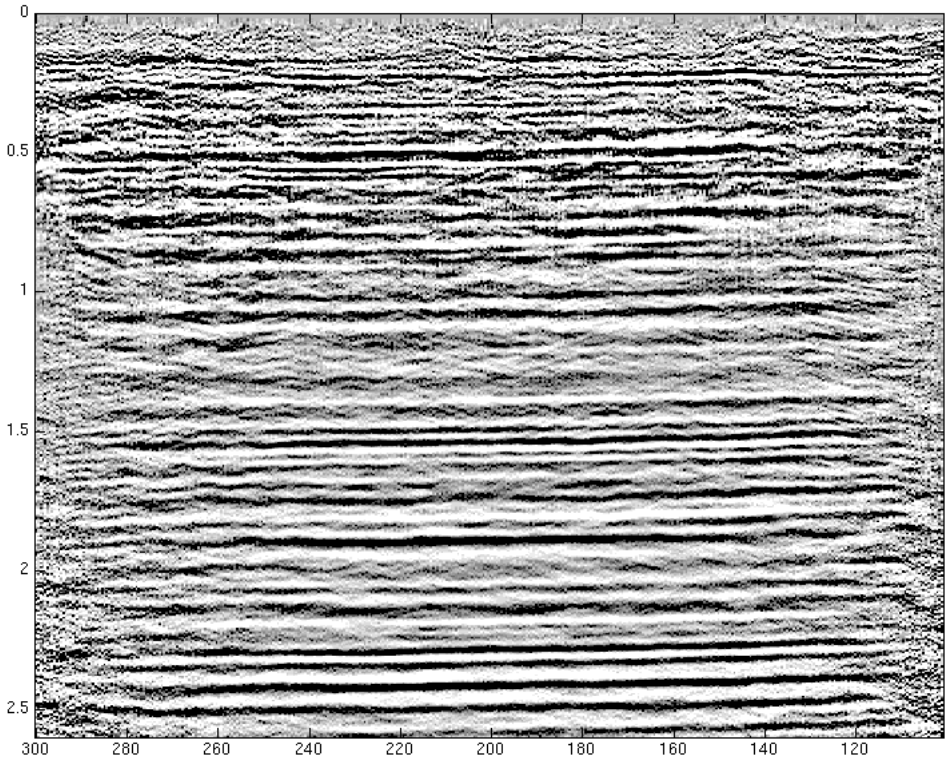

Fig. 5. Final stack 10 Hz radial component.

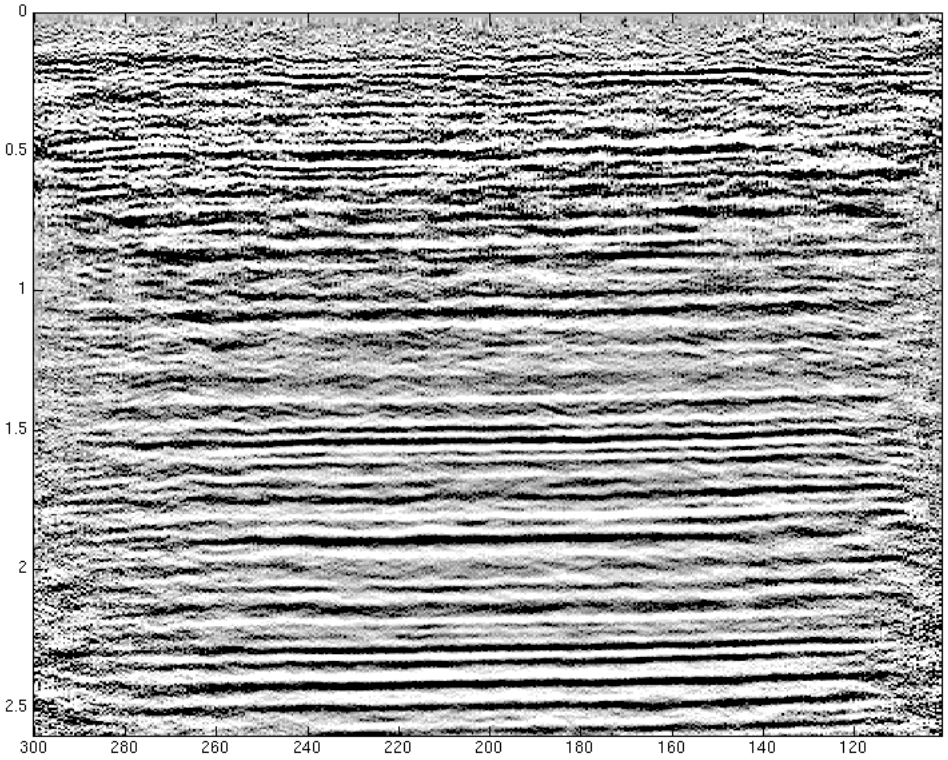

Fig. 6. Final stack 4.5 Hz radial component.

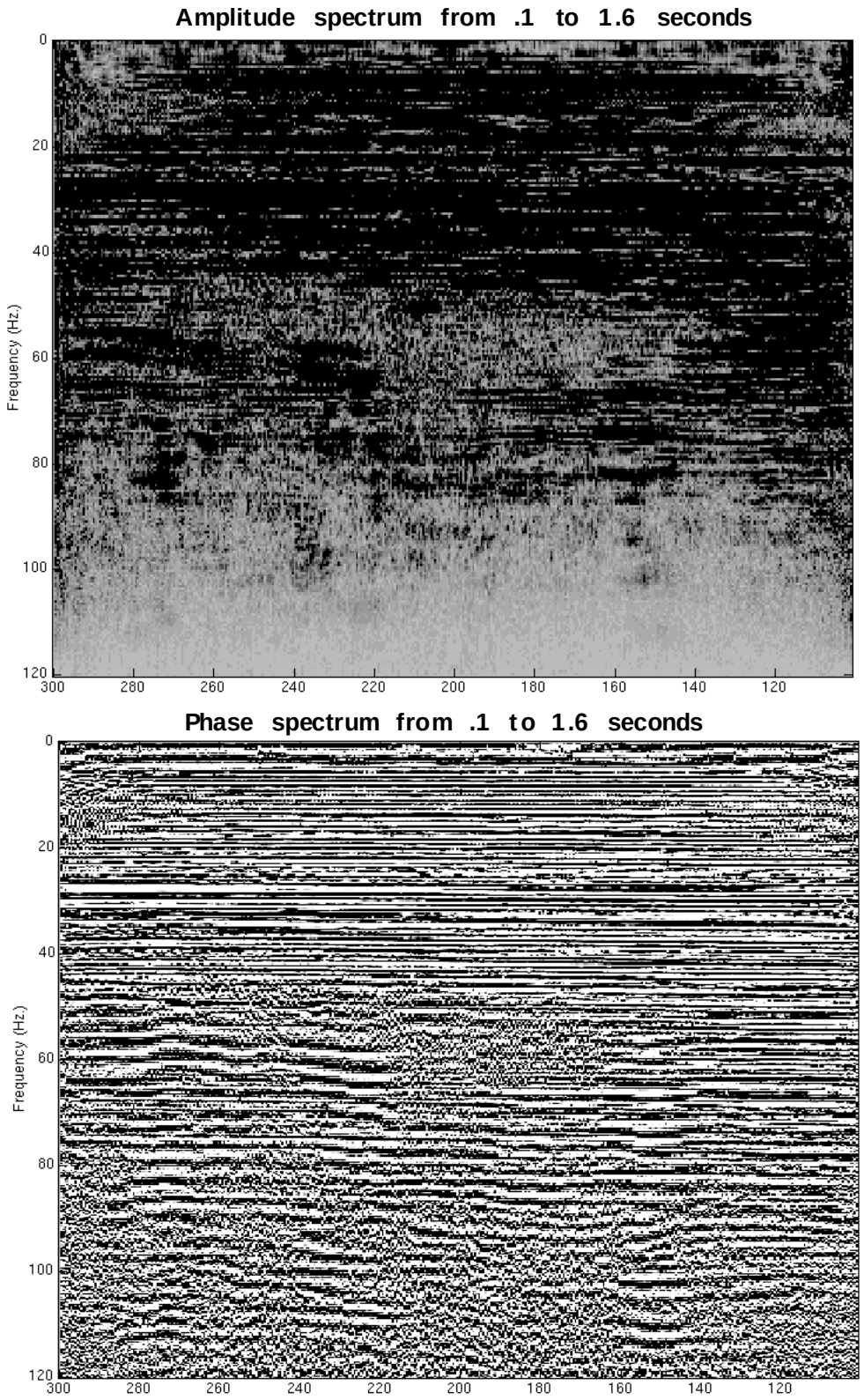

Fig. 7. f-x spectra of final stack of 10 Hz

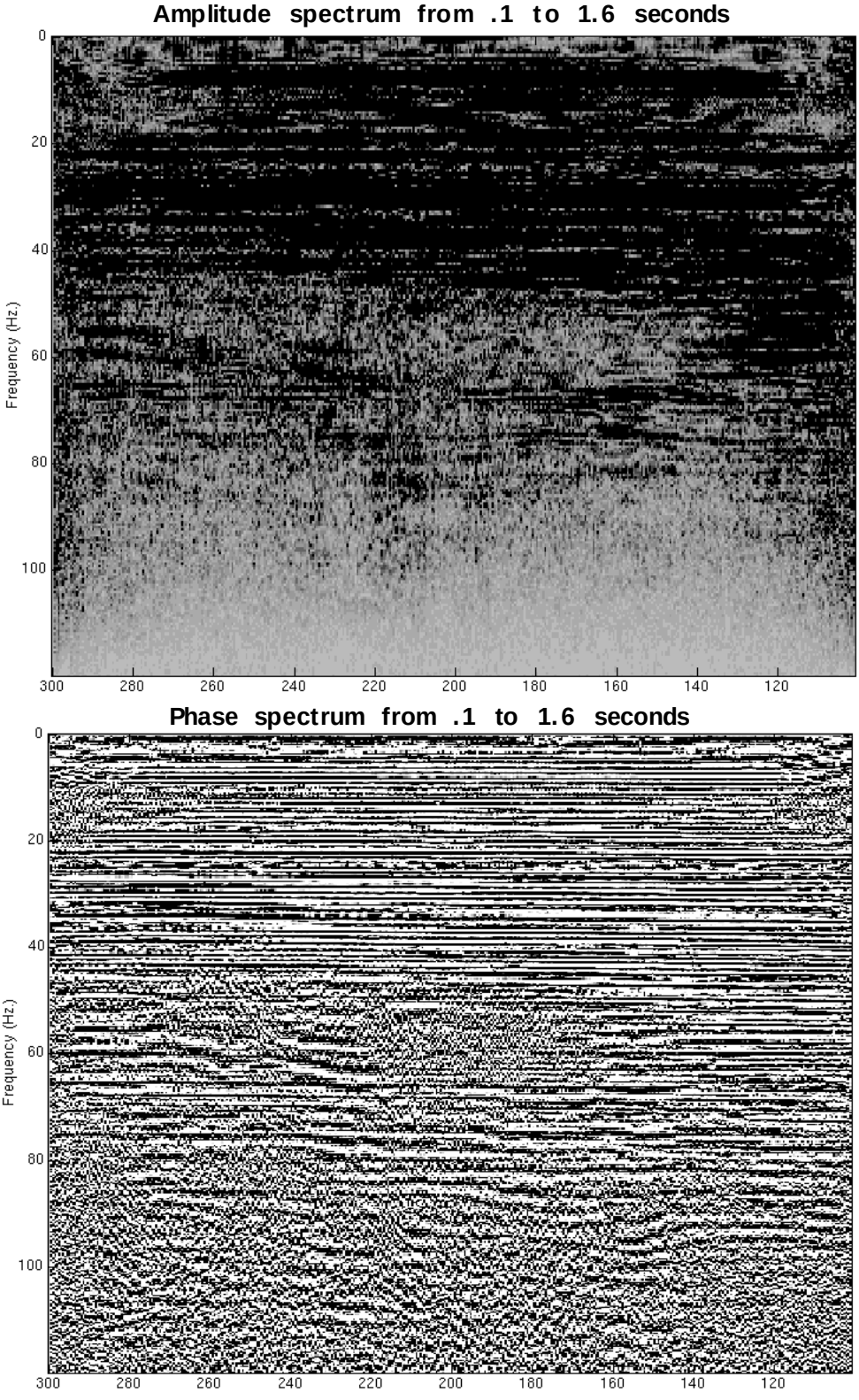

array.

Fig. 8. f-x spectra of final stack of 10 Hz vertical component.

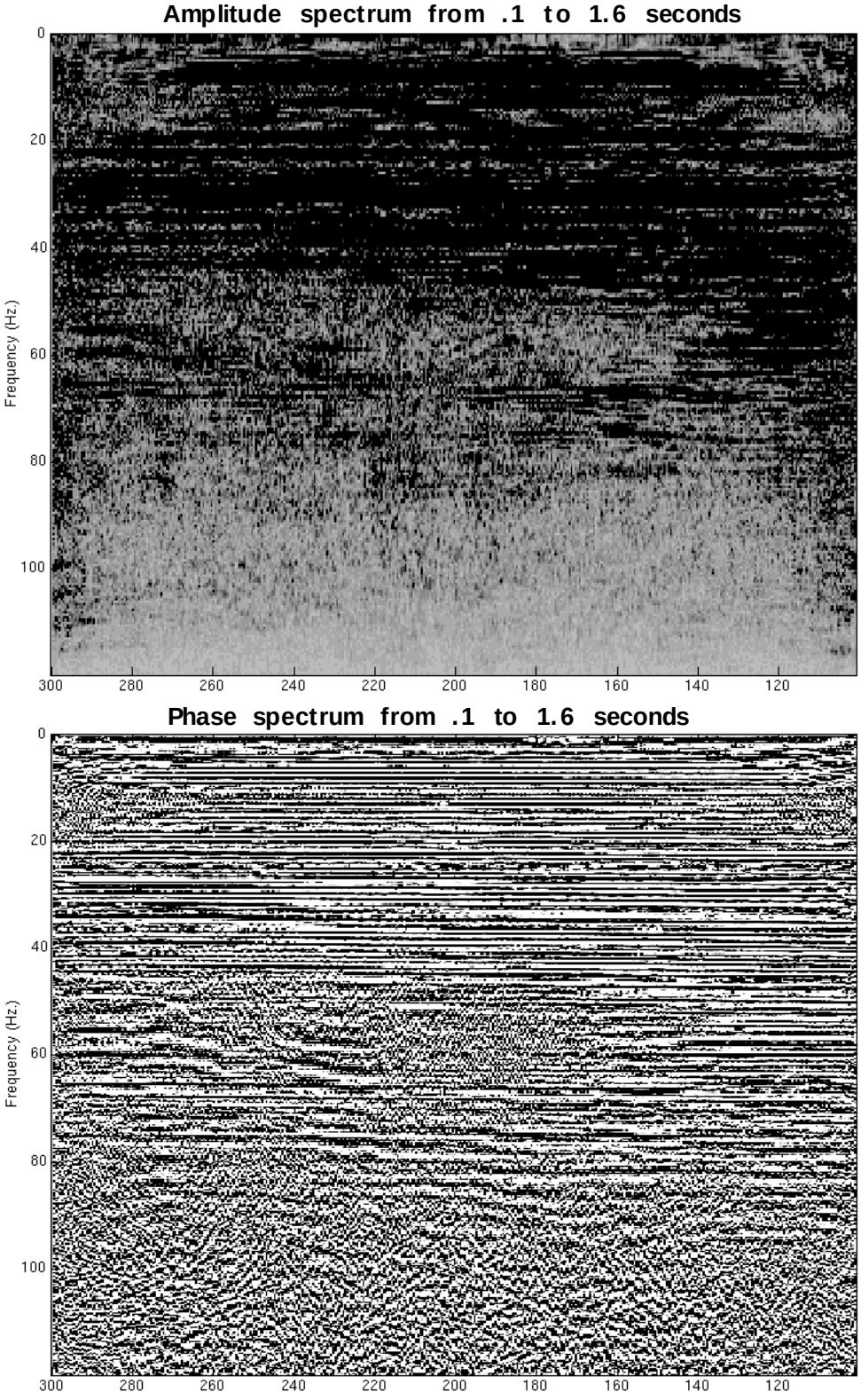

Fig. 9. f-x spectra of final stack of 4.5 Hz vertical component.

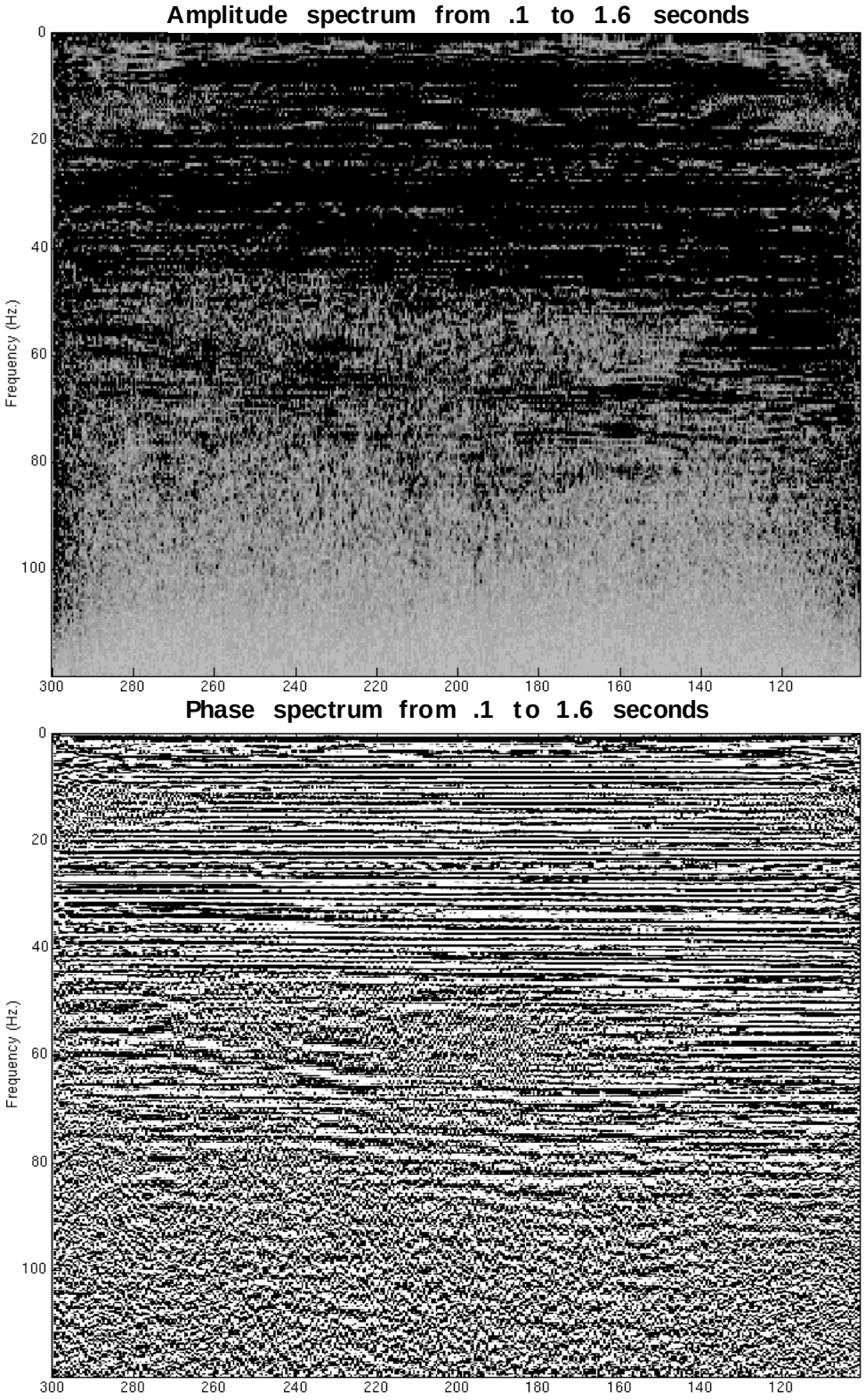

Fig. 10. f-x spectra of final stack of 2 Hz vertical component.

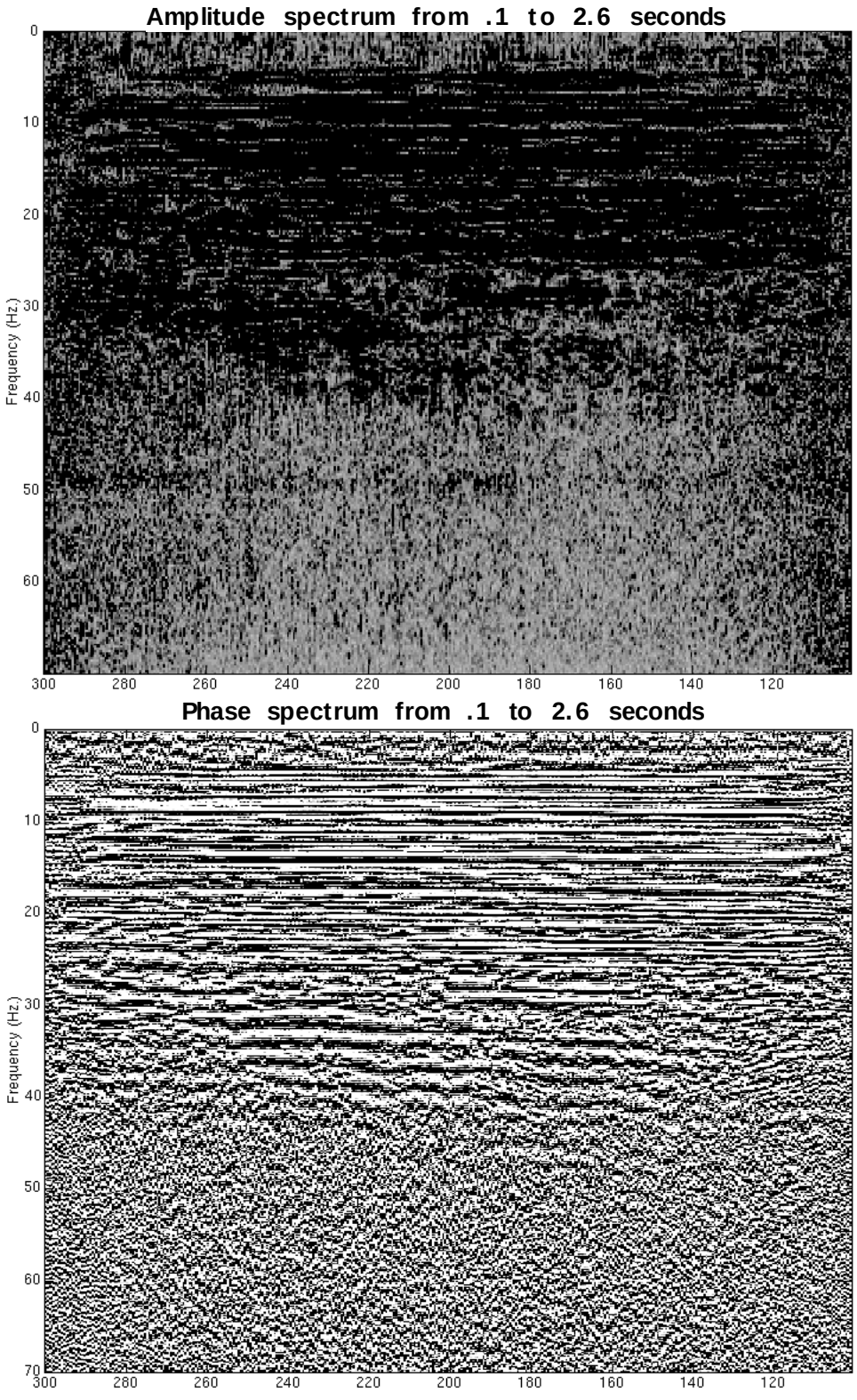

Fig. 11. f-x spectra of final stack of 10 Hz radial component.

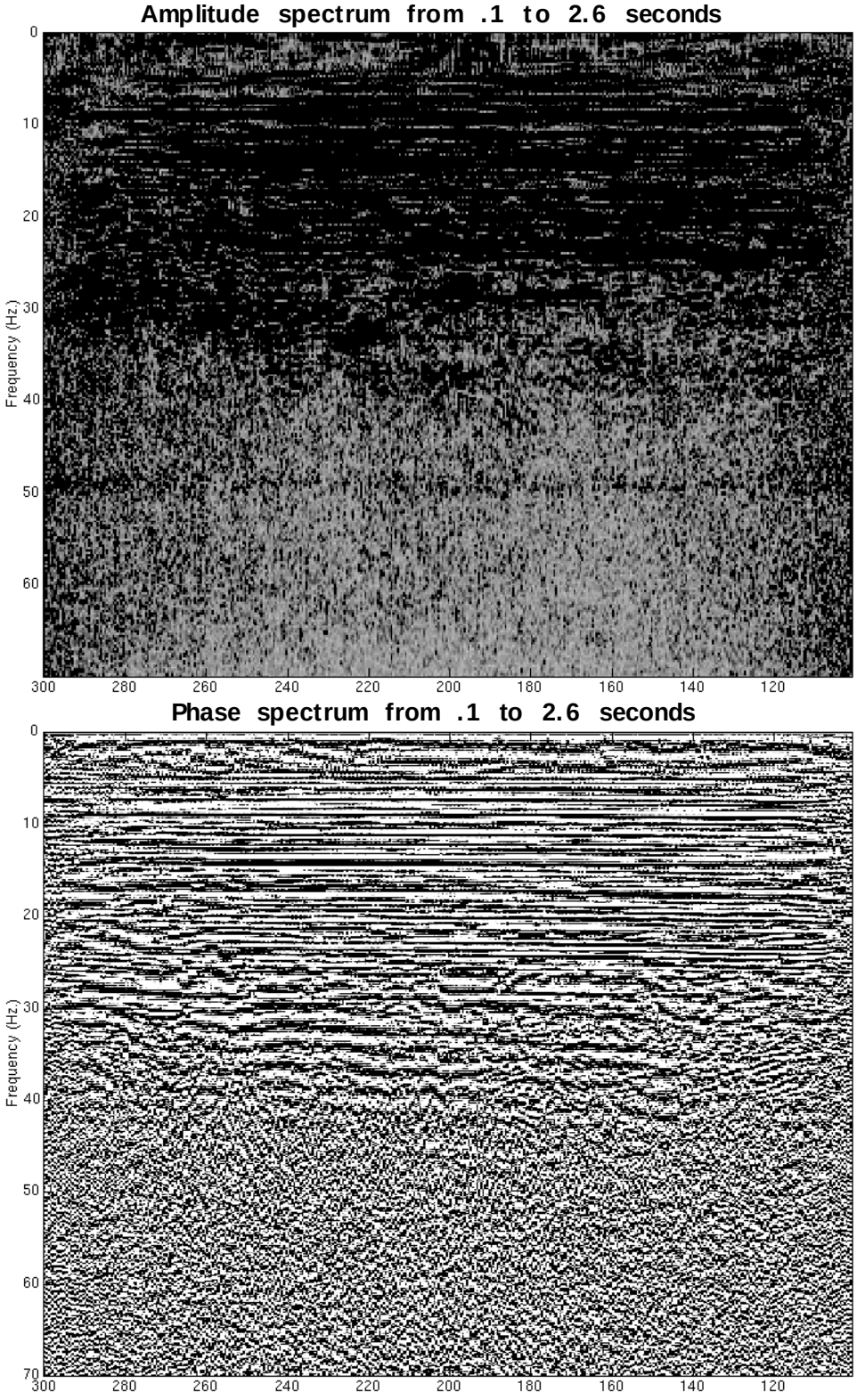

Fig. 12. f-x spectra of final stack of 4.5 Hz radial component.

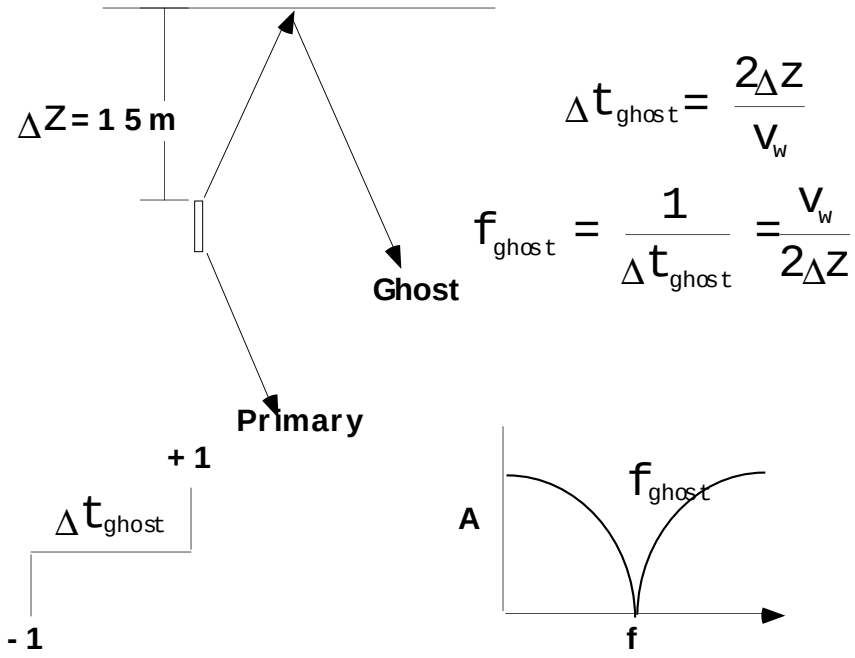

Fig. 13. A surface ghost causes a spectral notch.

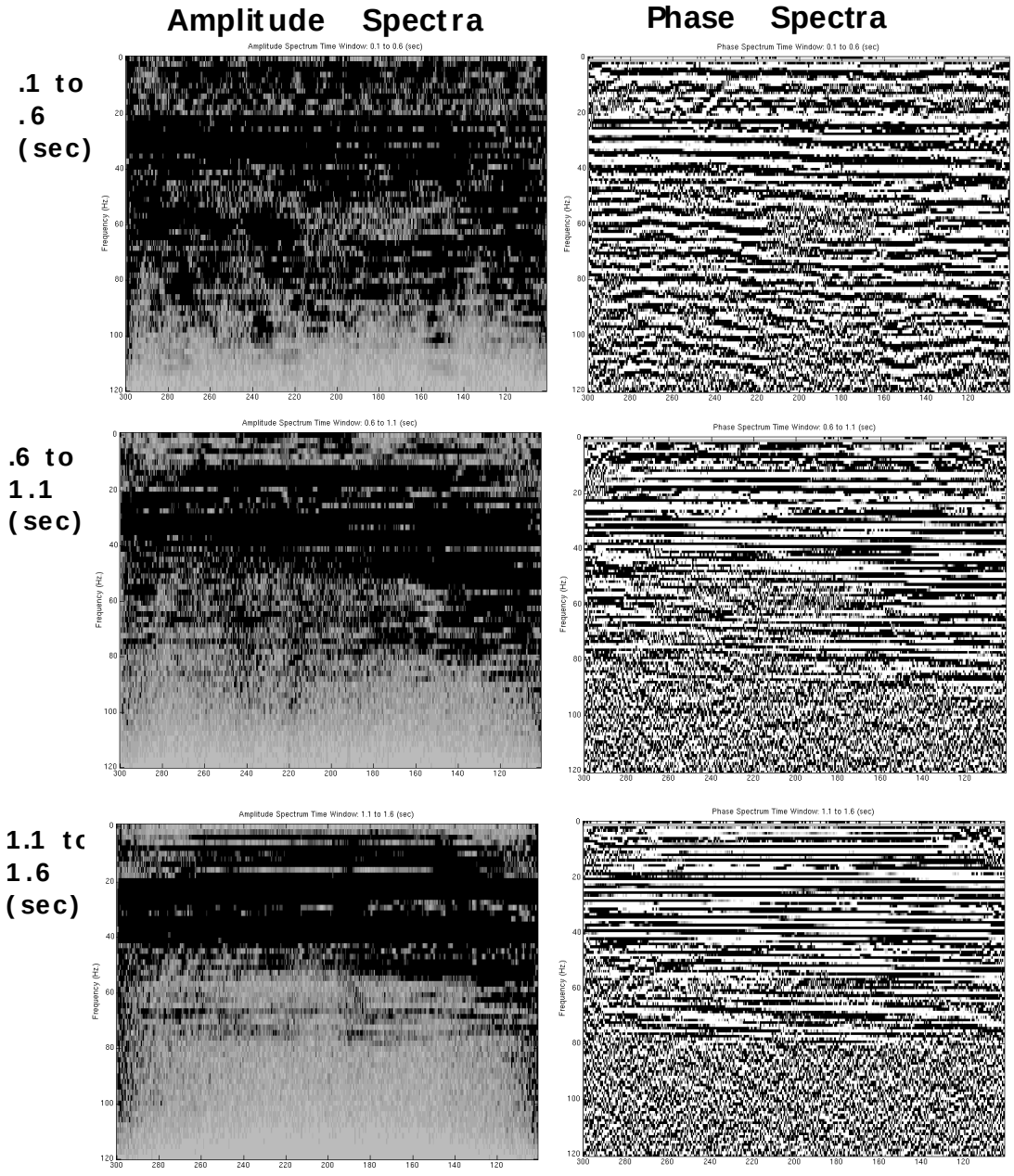

Fig. 14. f-x spectra from three different time windows on final stack of 10 Hz vertical array

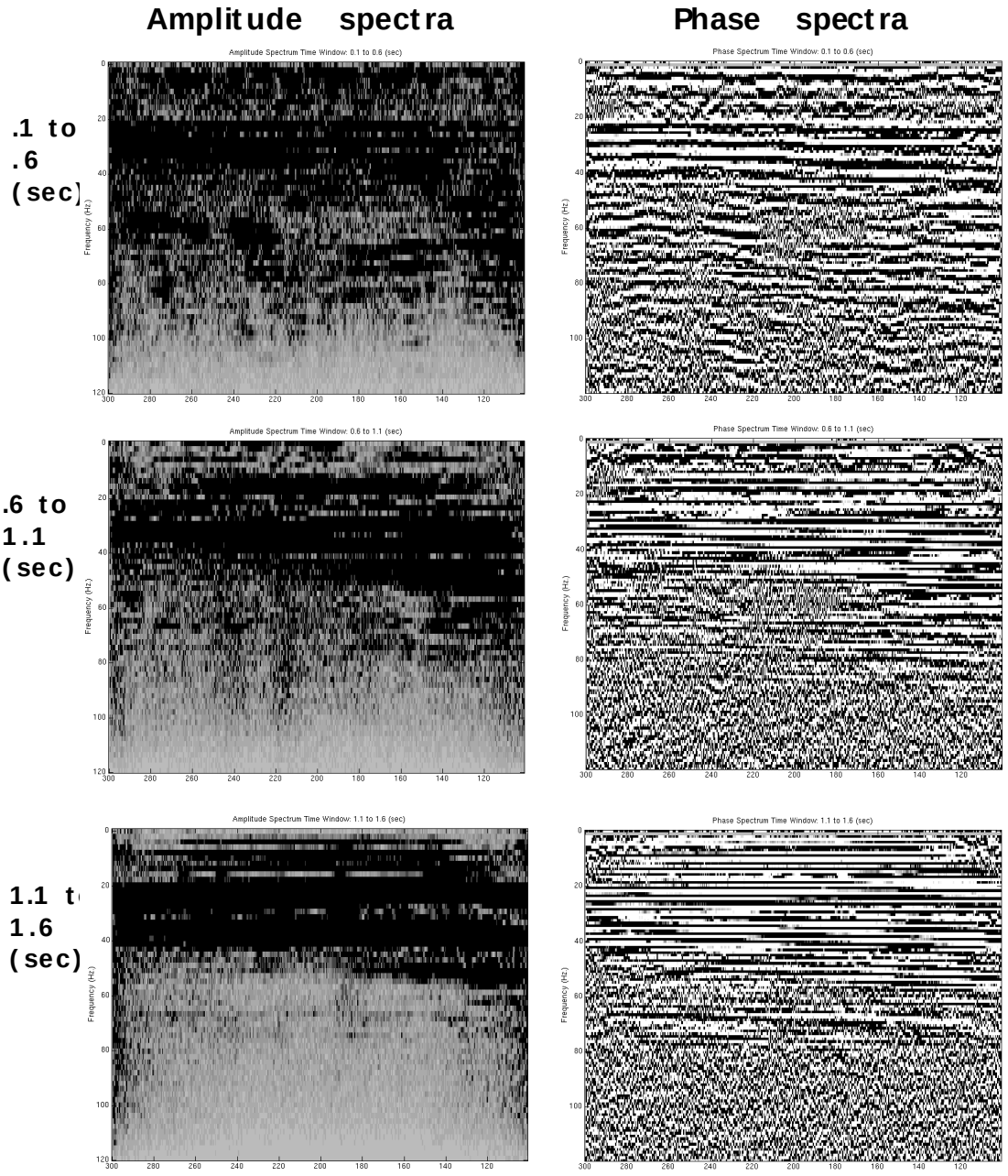

Fig. 15. f-x spectra from three different time windows on final stack of 10 Hz vertical component

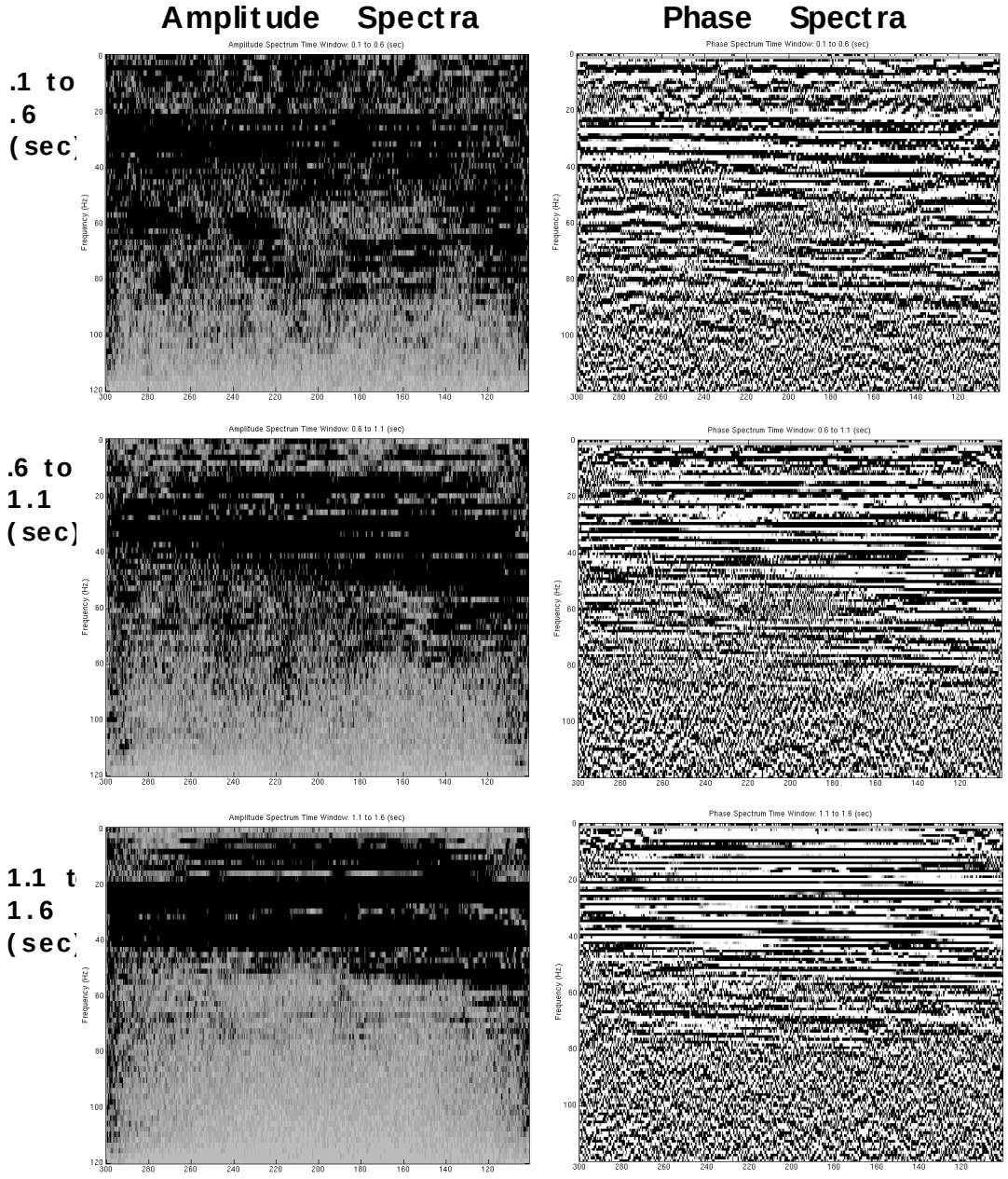

Fig. 16. f-x spectra from three different time windows on final stack of 4.5 Hz vertical component

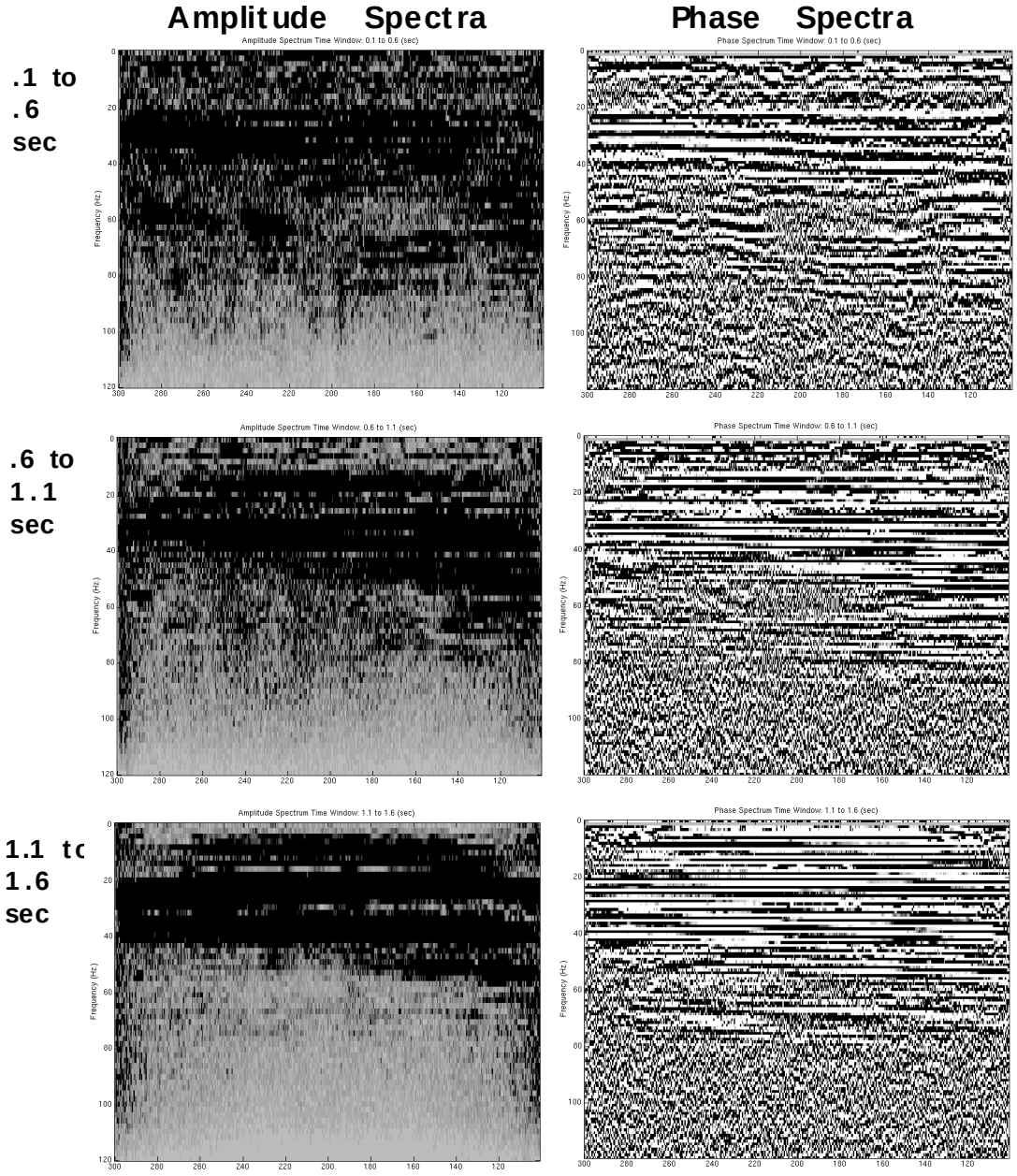

Fig. 17. f-x spectra from three different time windows on final stack of 2 Hz vertical component

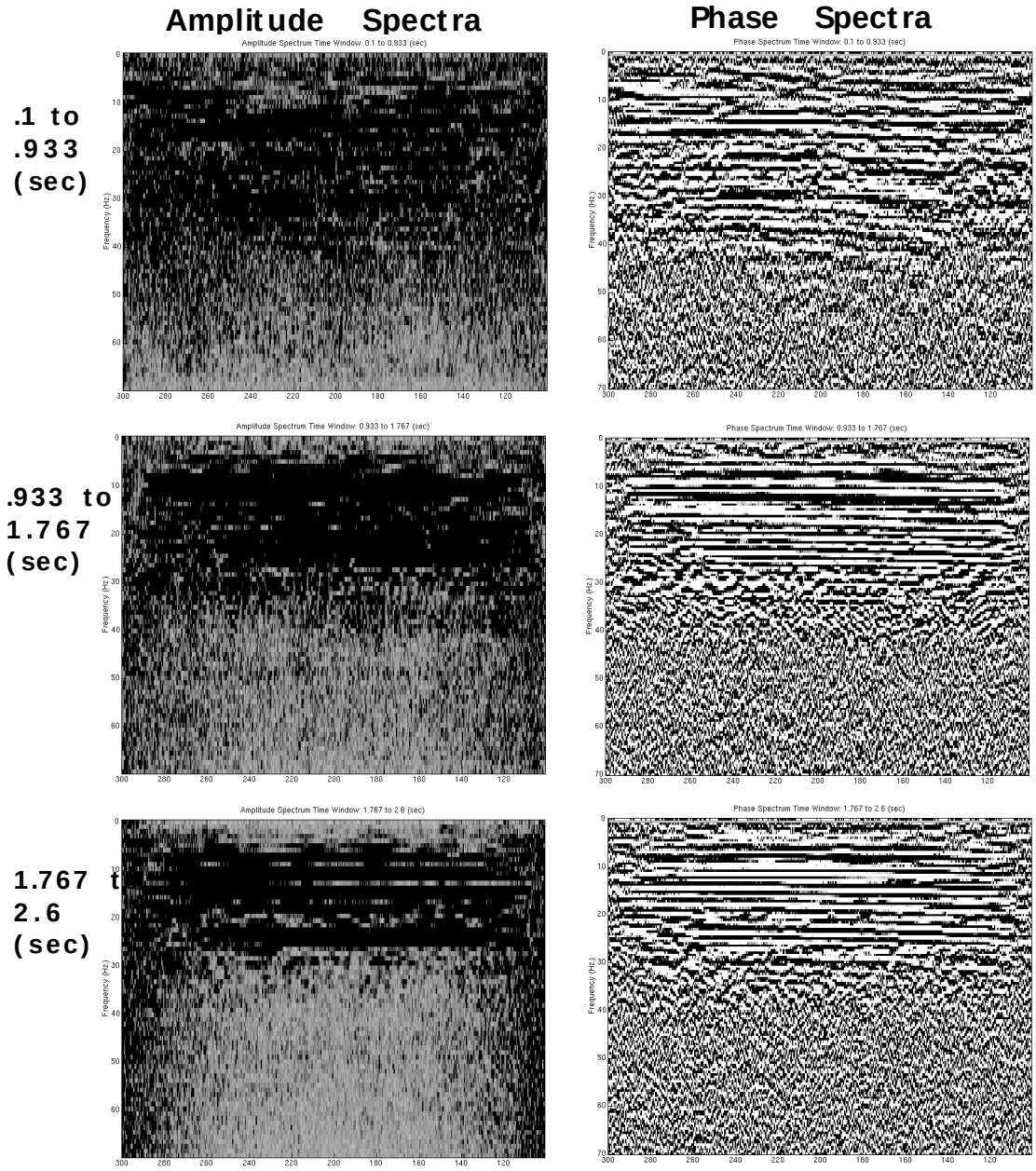

Fig. 18. f-x spectra from three different time windows on final stack of 10 Hz radial component

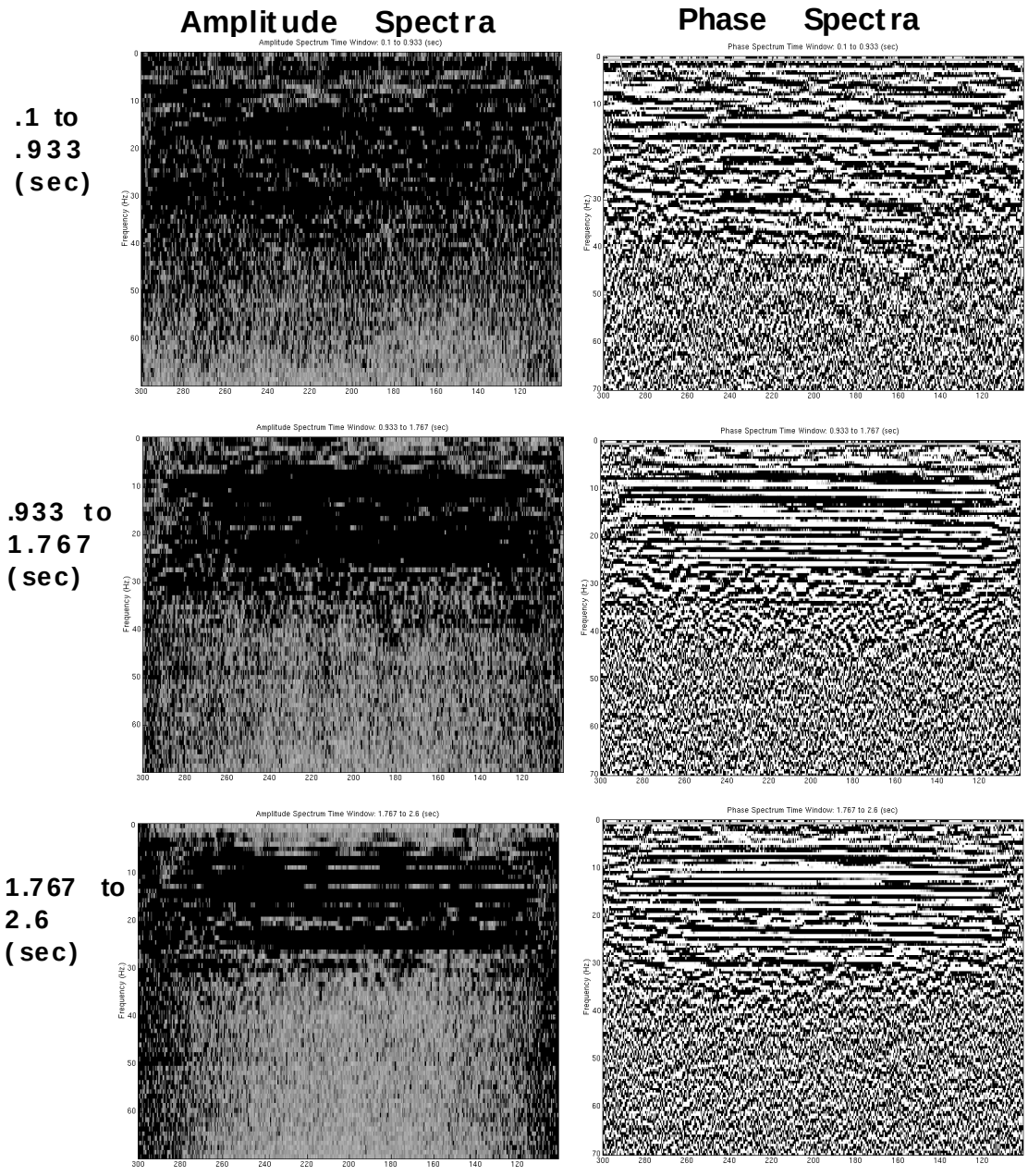

Fig. 19. f-x spectra from three different time windows on final stack of 4.5 Hz radial component

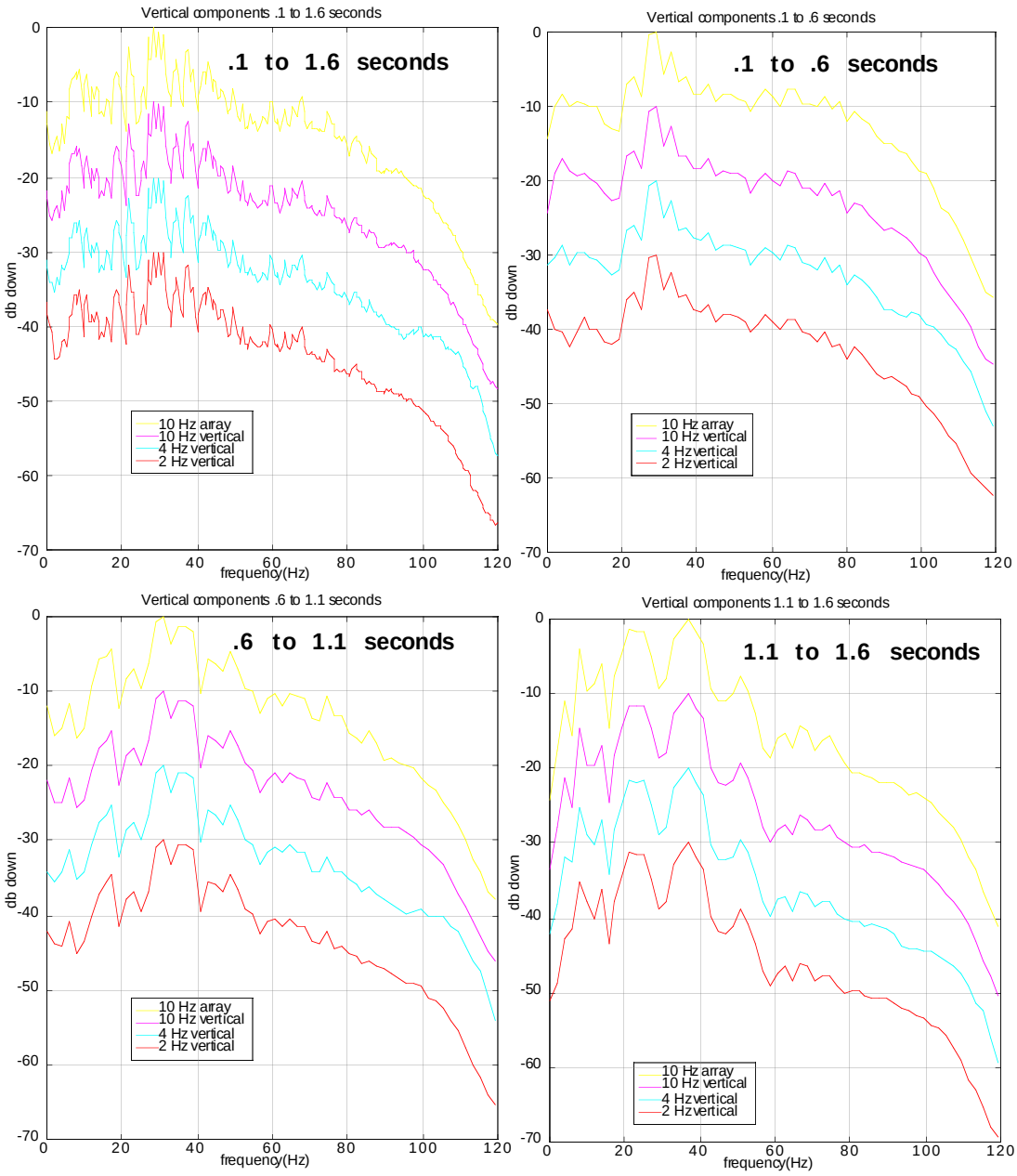

Fig. 20. Average amplitude spectra taken from vertical component final stacks.

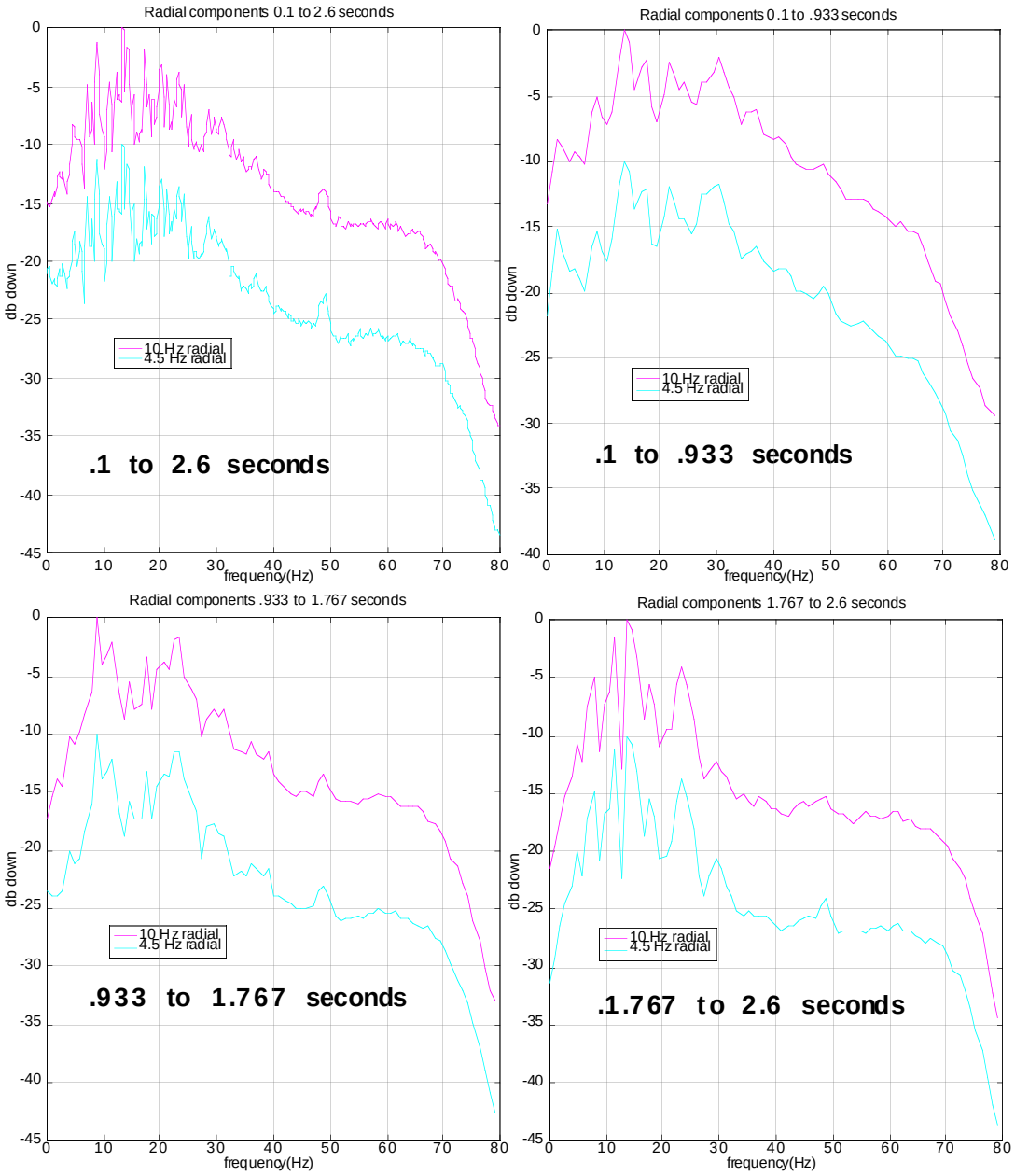

Fig. 21. Average amplitude spectra taken from vertical component final stacks.

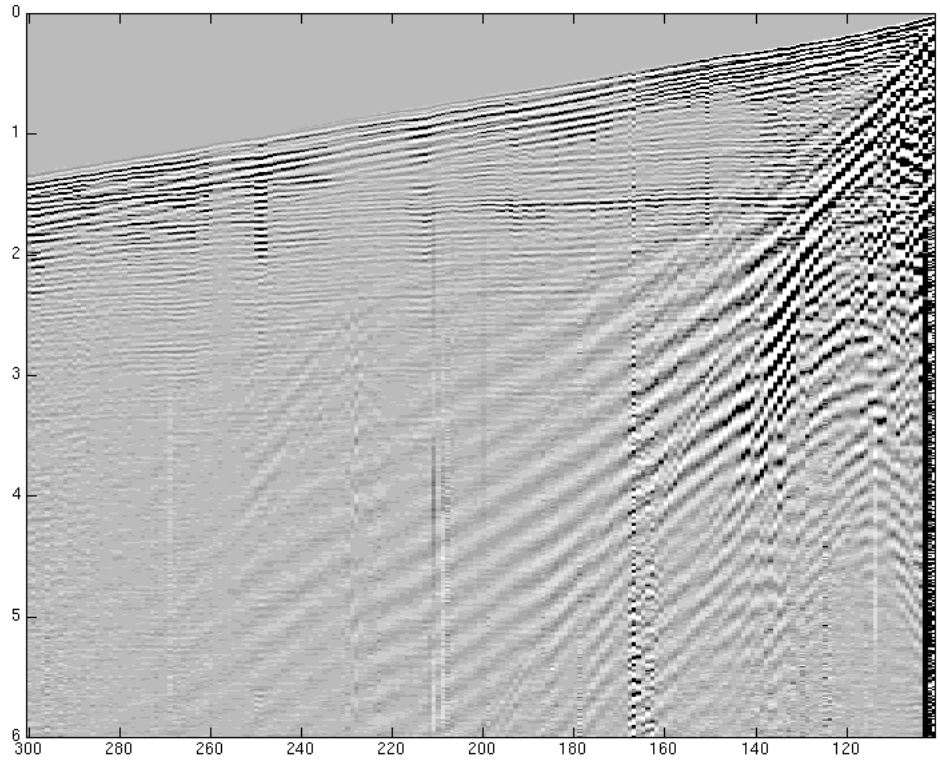

Fig. 22. Shot 101 10 Hz array.

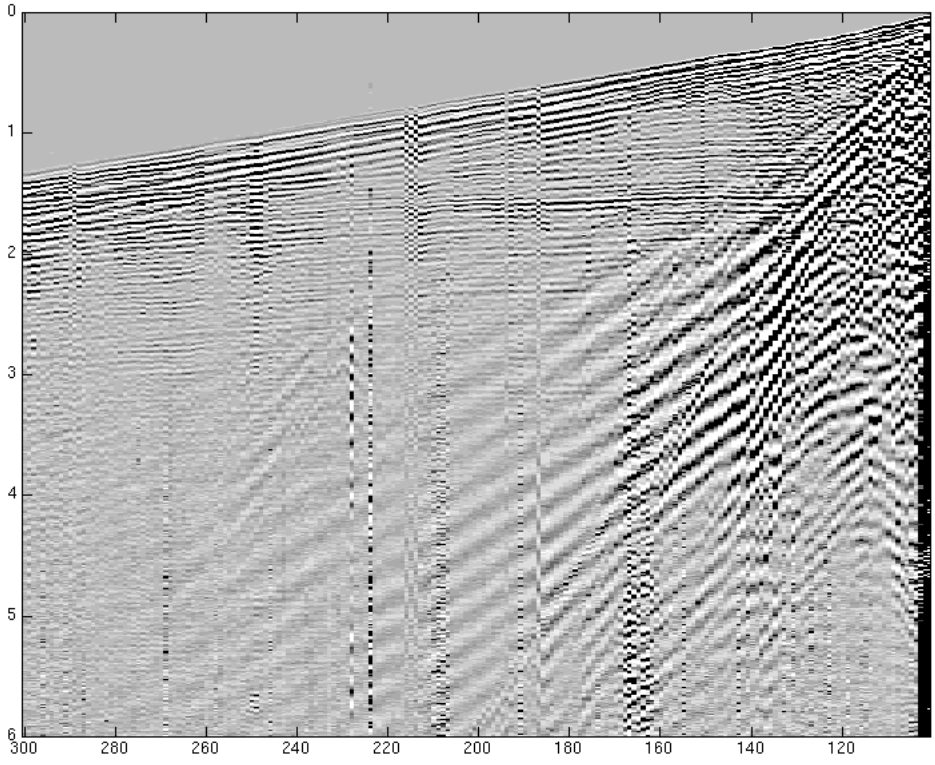

Fig. 23 Shot 101 10 Hz vertical component.

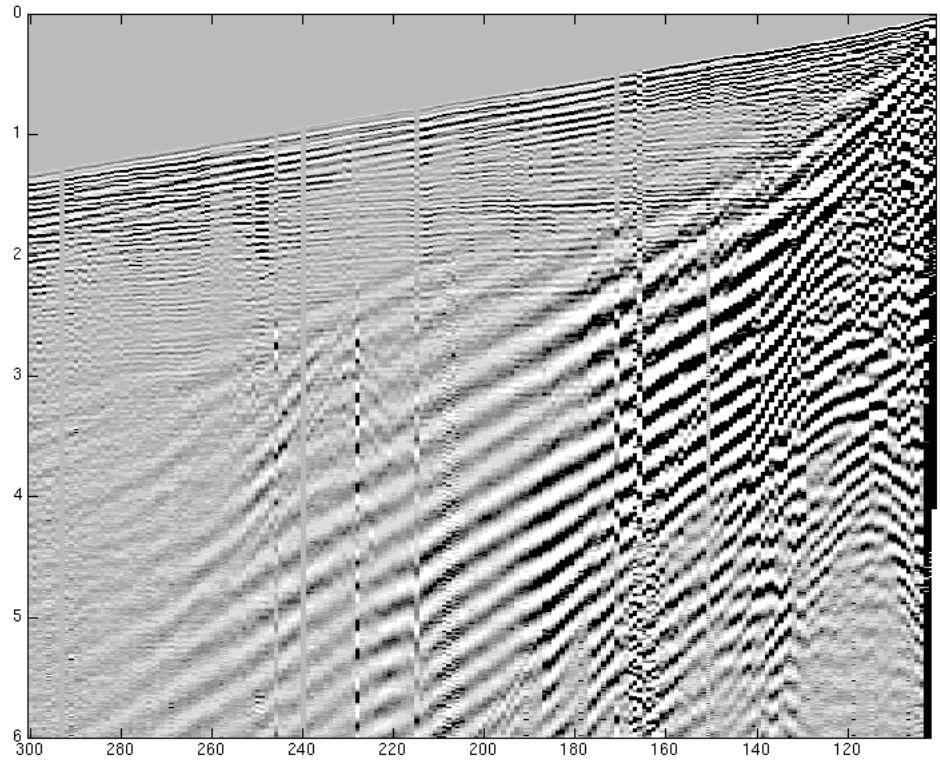

Fig. 24. Shot 101 4.5 Hz vertical component.

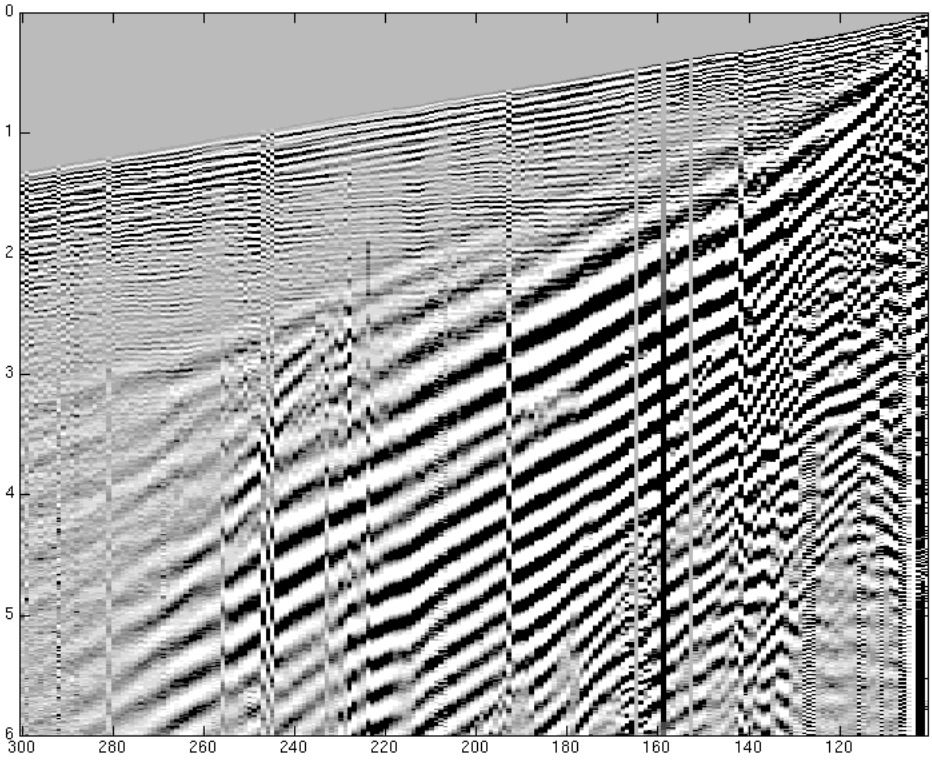

Fig. 25. Shot 101 2 Hz vertical component

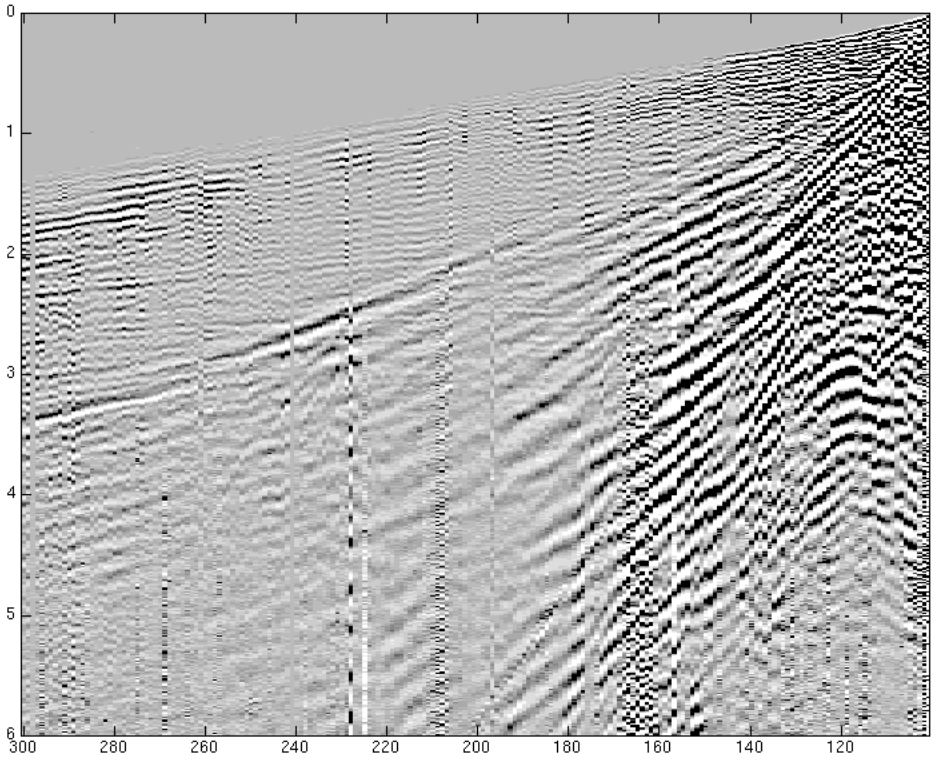

Fig. 26. Shot 101 10 Hz radial component

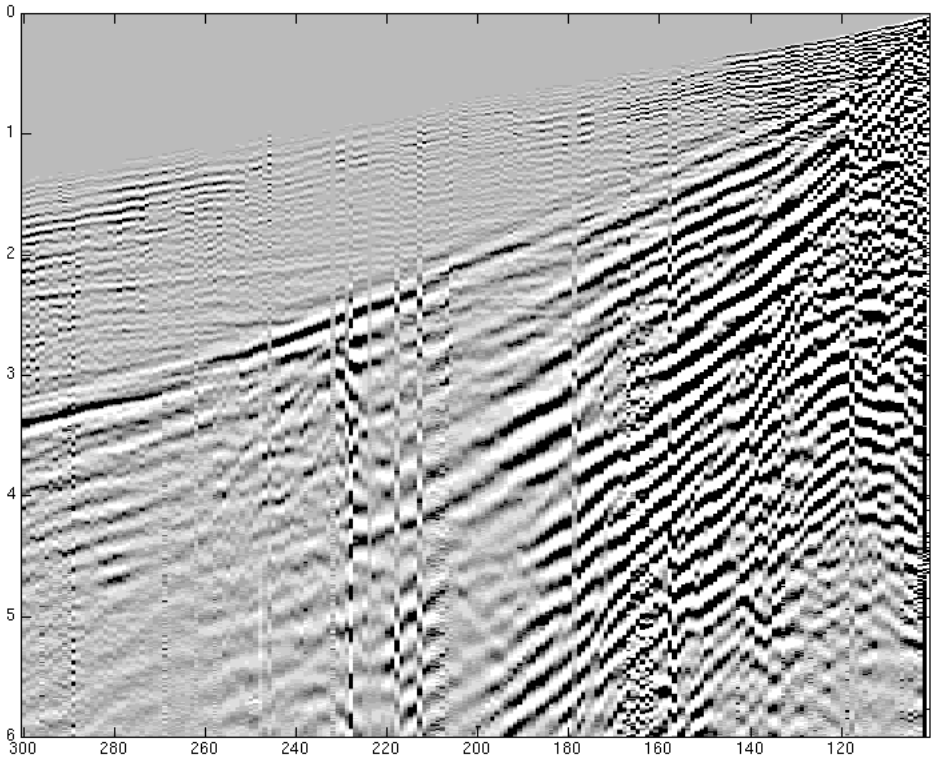

Fig. 27. Shot 101 4.5 Hz radial component

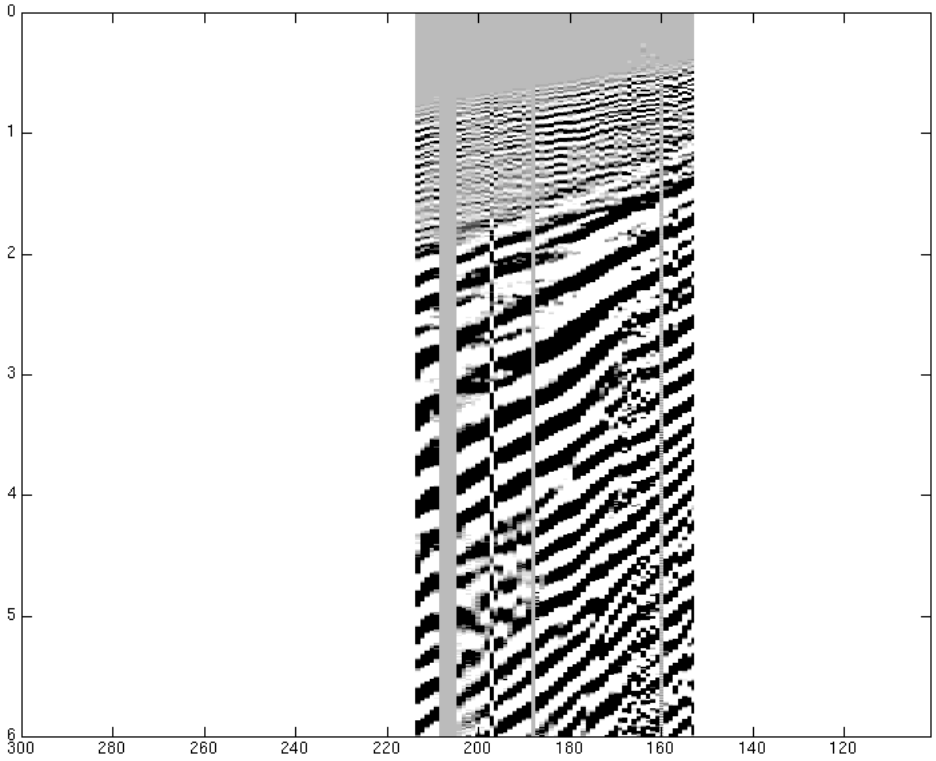

Fig. 28. Shot 101 2 Hz radial component

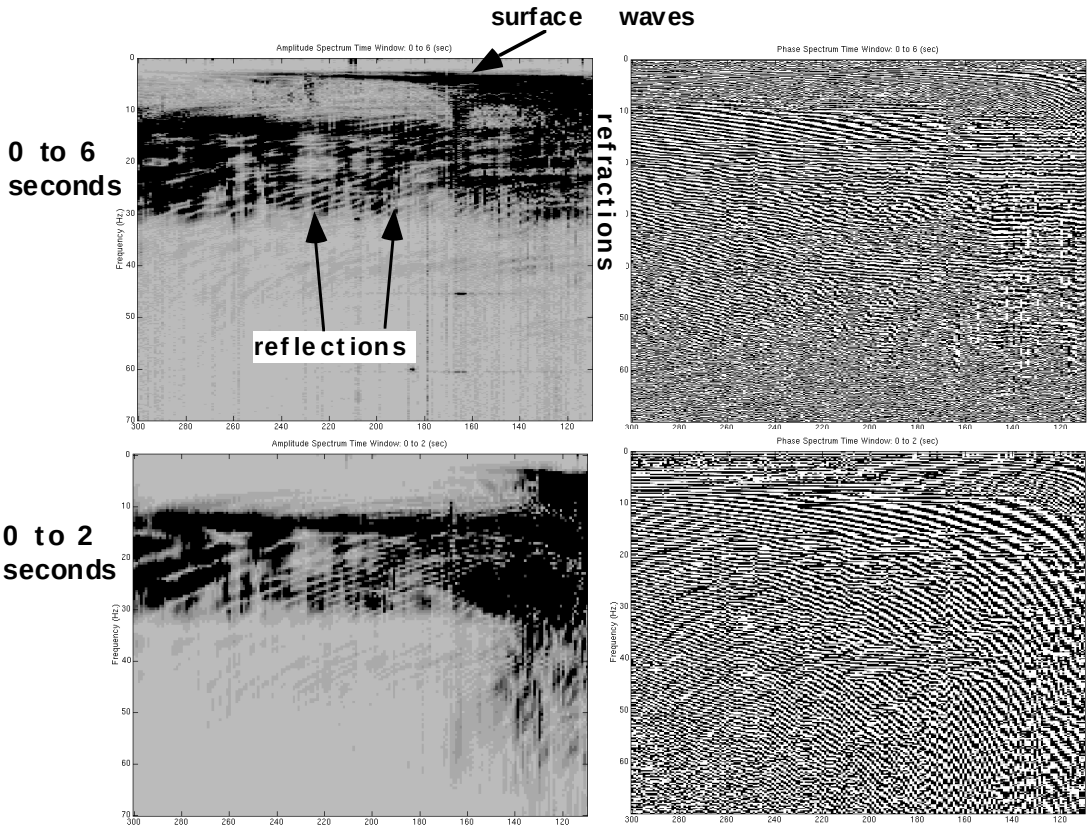

Fig. 29 f-x spectra from shot 101 10 Hz array.

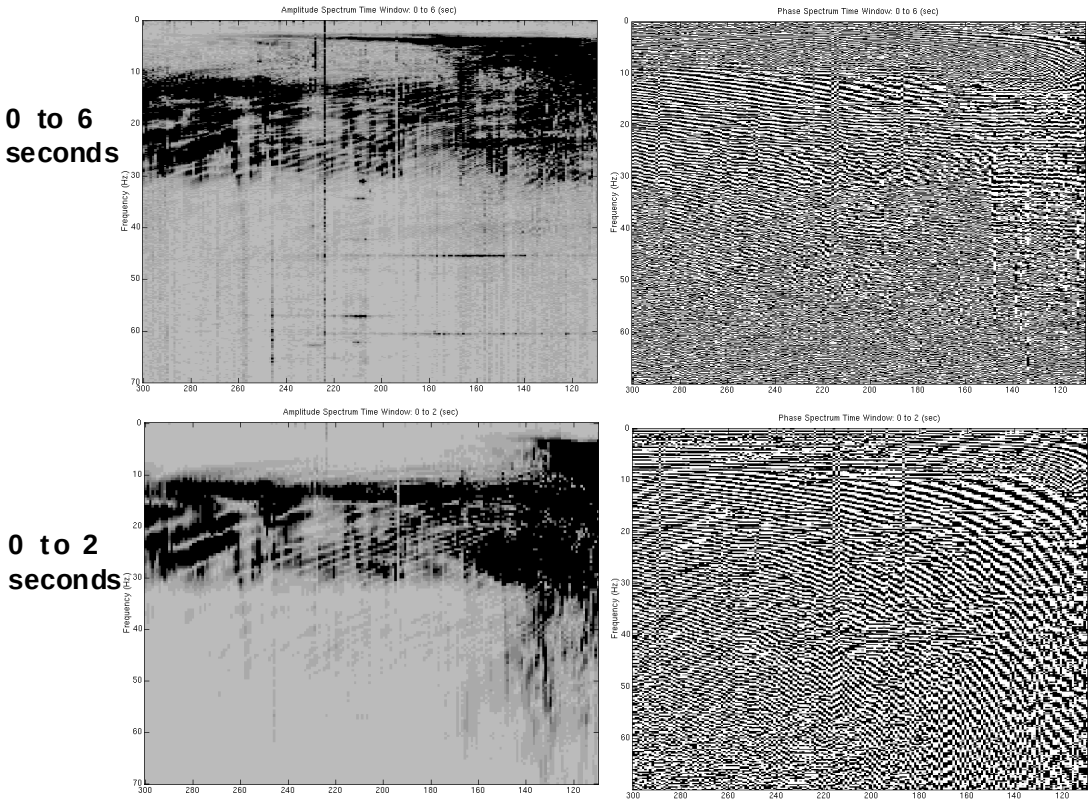

Fig. 30 f-x spectra from shot 101 10 Hz vertical component.

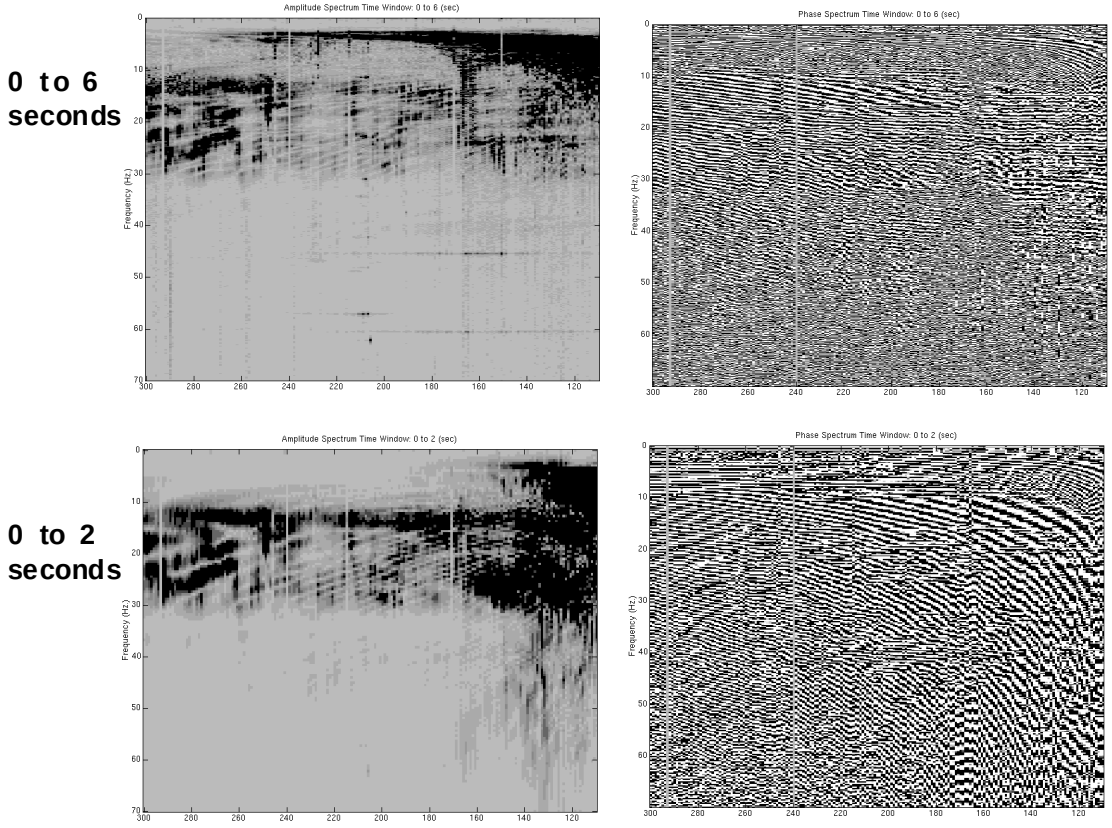

Fig. 31 f-x spectra from shot 101 4.5 Hz array.

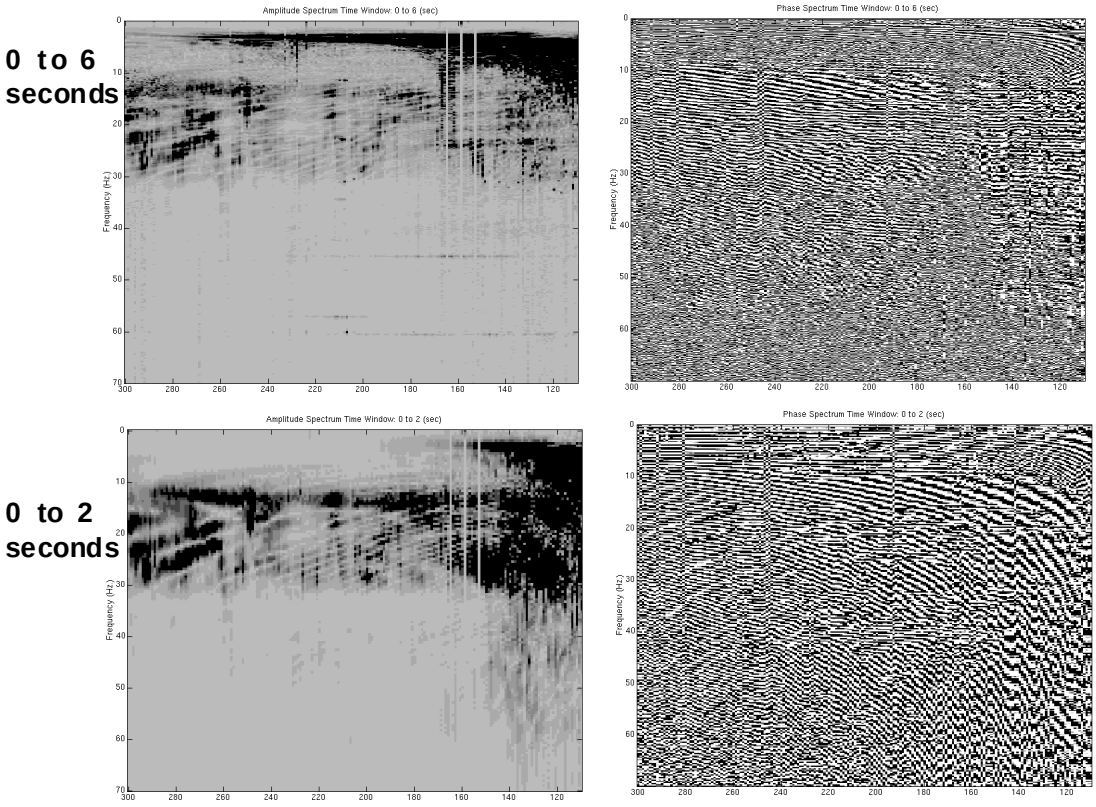

Fig. 32. f-x spectra from shot 101 2 Hz vertical component.

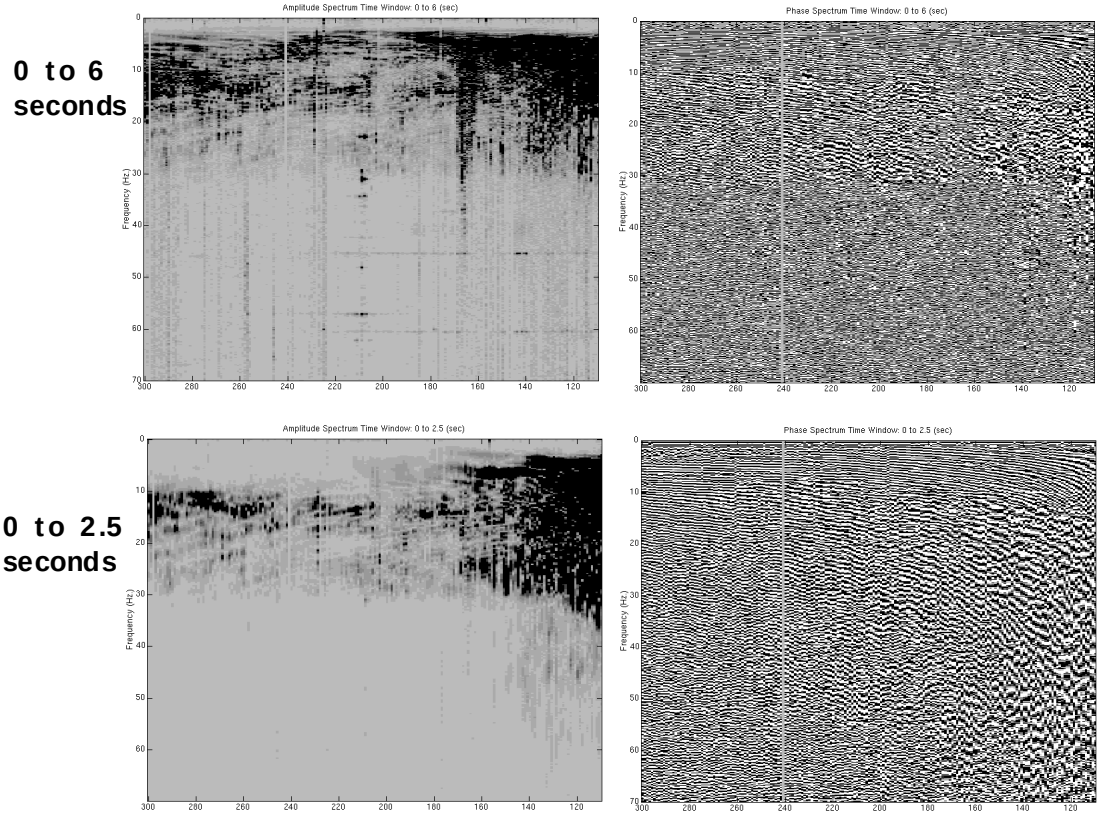

Fig. 33. f-x spectra from shot 101 10 Hz radial component.

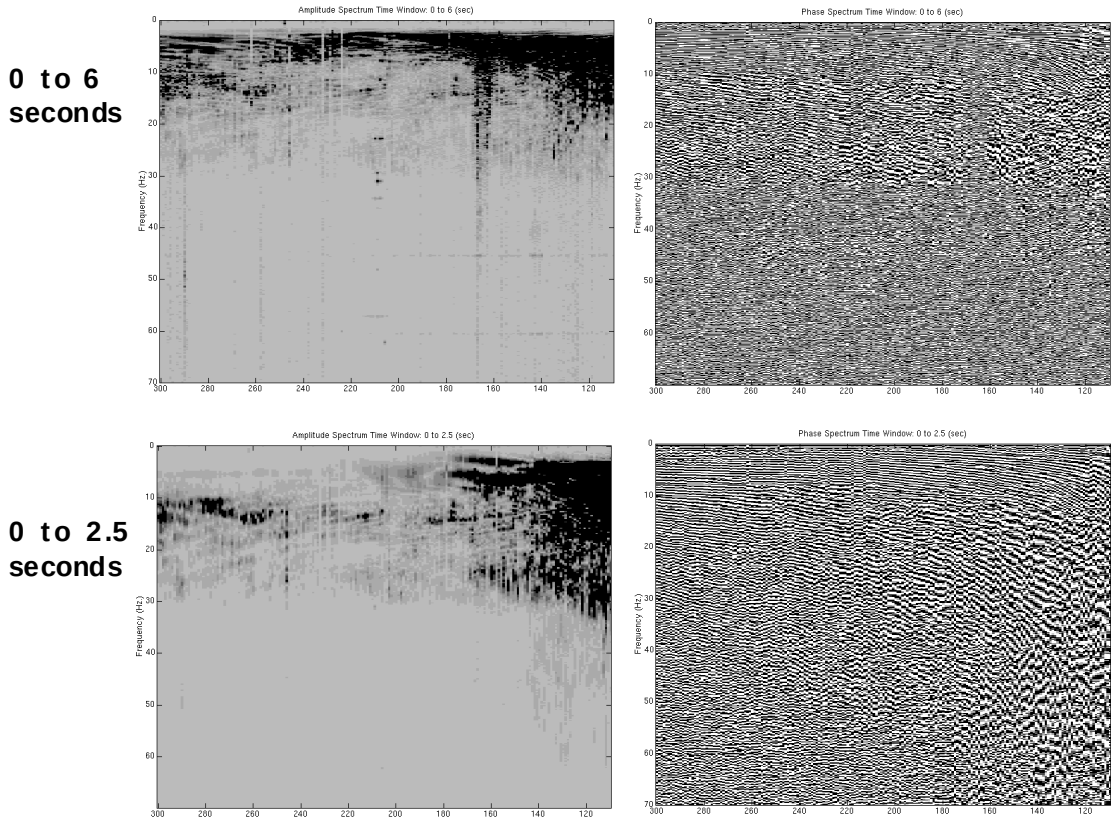

Fig. 34. f-x spectra from shot 101 4.5 Hz radial component.

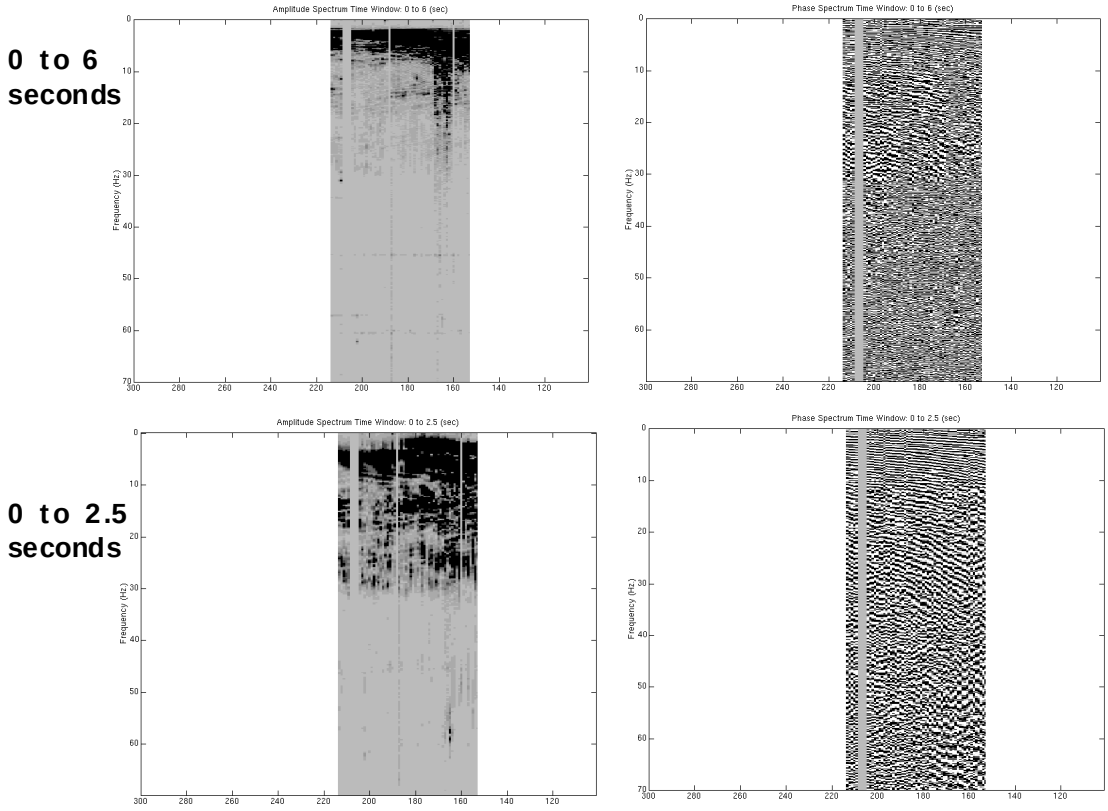

Fig. 35. f-x spectra from shot 101 2 Hz radial component.

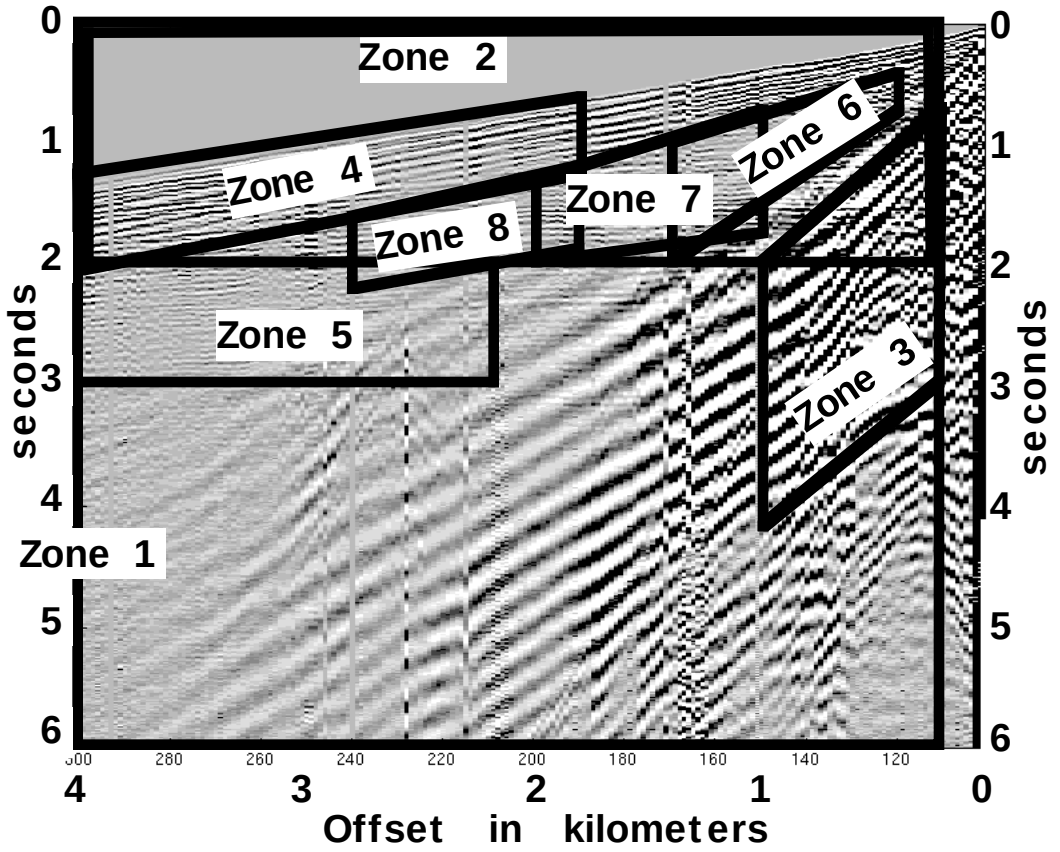

Zone	x1 & x2	times(x1)	times(x2)	comments
1	110 300	0 6	0 6	total record
2	110 300	0 2	0 2	mostly above basement
3	110 150	.75 3	2 4.25	surface waves
4	190 300	.6 1.25	1.25 2.1	first breaks
5	210 300	2 3	2 3	reflections below bsmt
6	120 170	.4 .75	1 2	shallow reflections
7	150 200	.75 1.75	1.3 2.0	intermediate reflections
8	190 240	1.2 1.8	1.6 2.2	deep reflections

Fig. 36. Shot 101 vertical component spectral analysis zones shown on top of 4.5 Hz record.

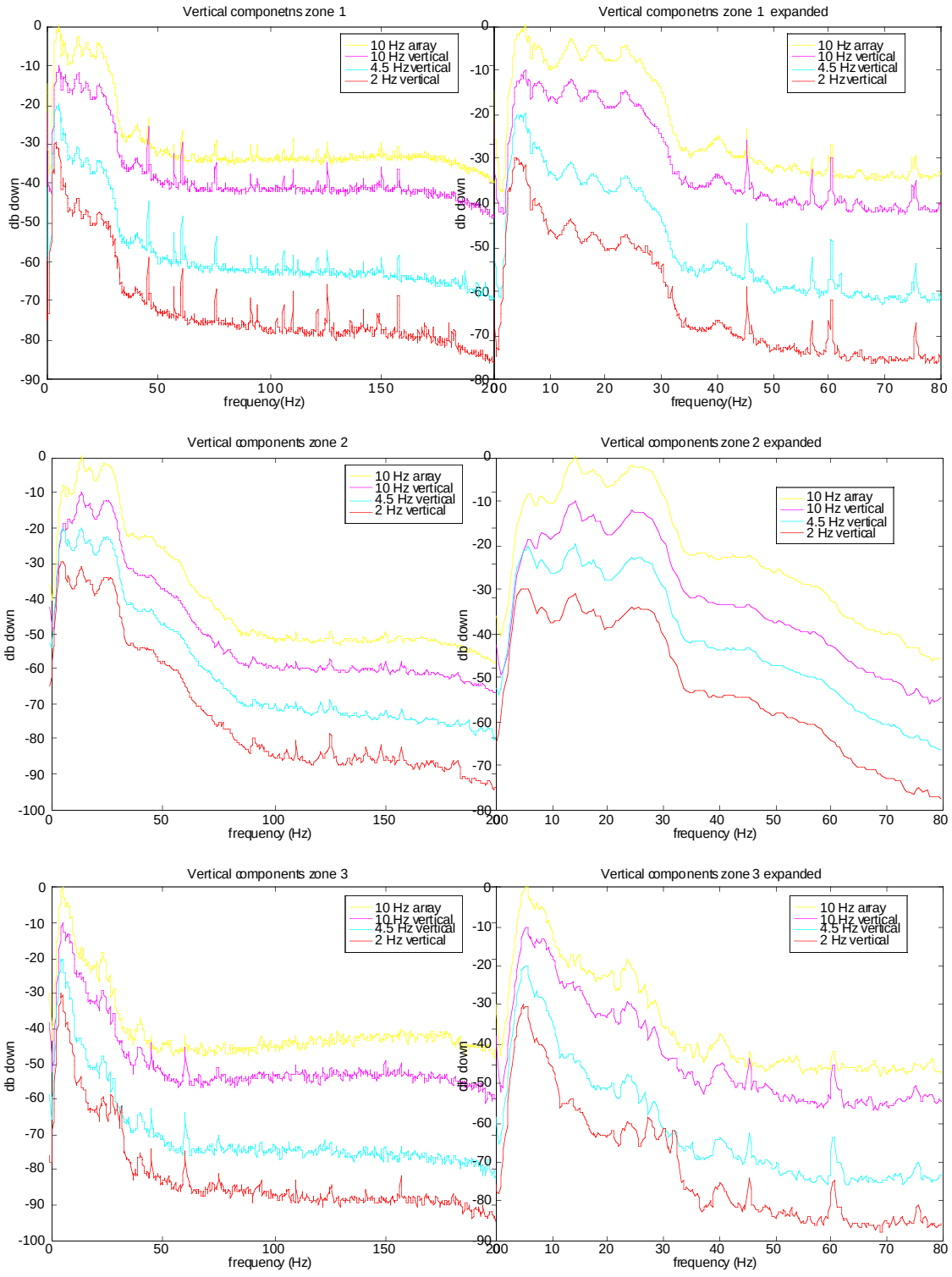

Fig. 36. Averaged amplitude spectra from shot 101 vertical component analysis zones 1-3 (see fig. 36)

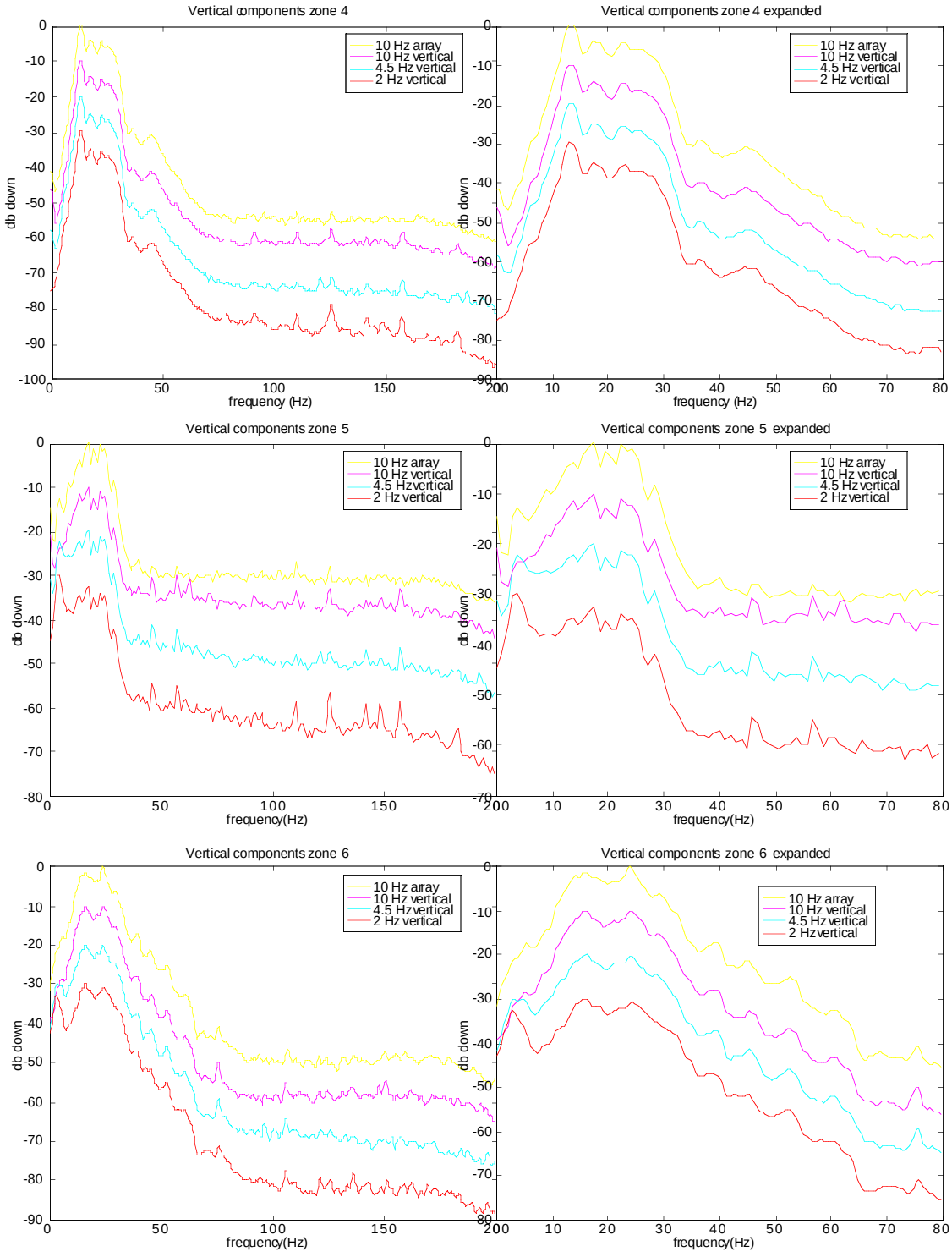

Fig. 38. Averaged amplitude spectra from shot 101 vertical component analysis zones 4-6 (see fig. 36)

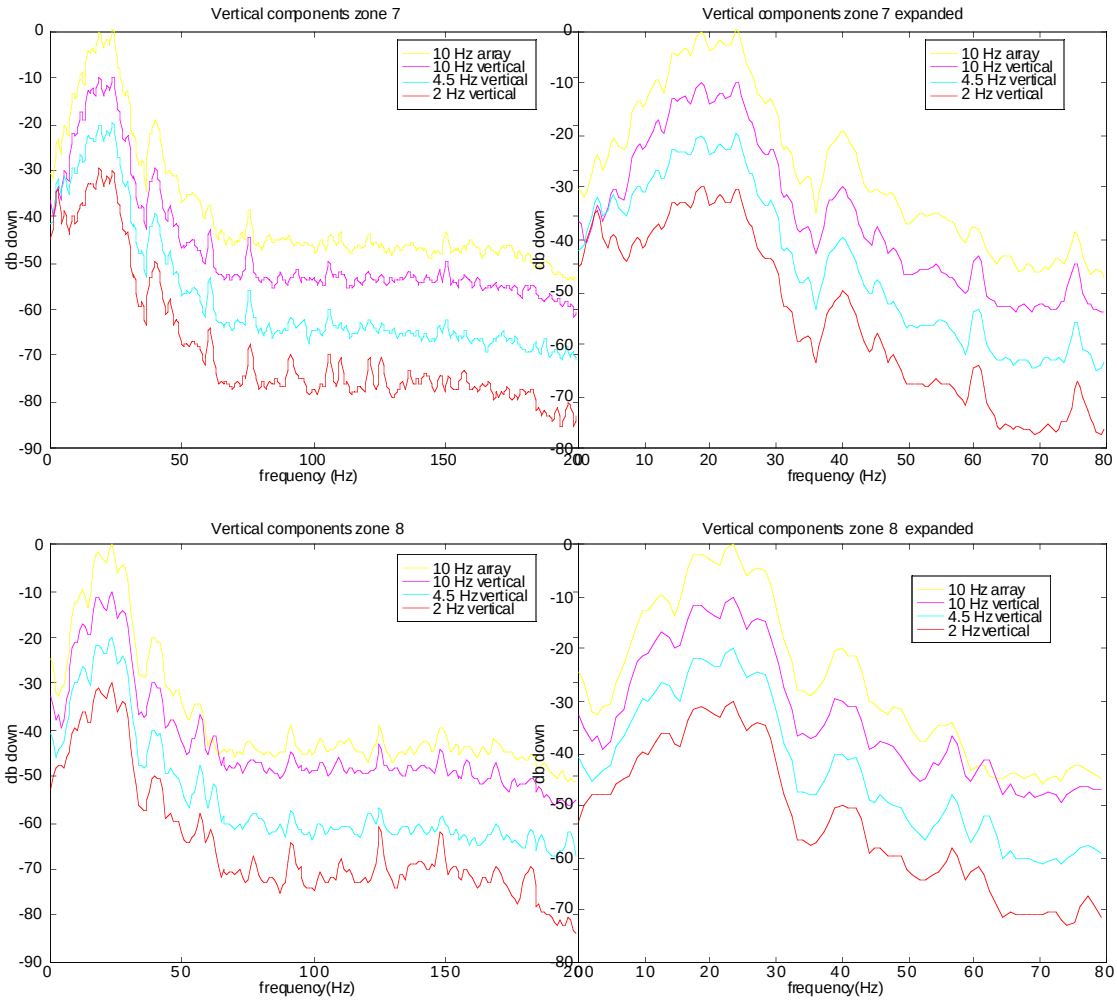

Fig. 39. Averaged amplitude spectra from shot 101 vertical component analysis zones 7-8 (see fig. 36)

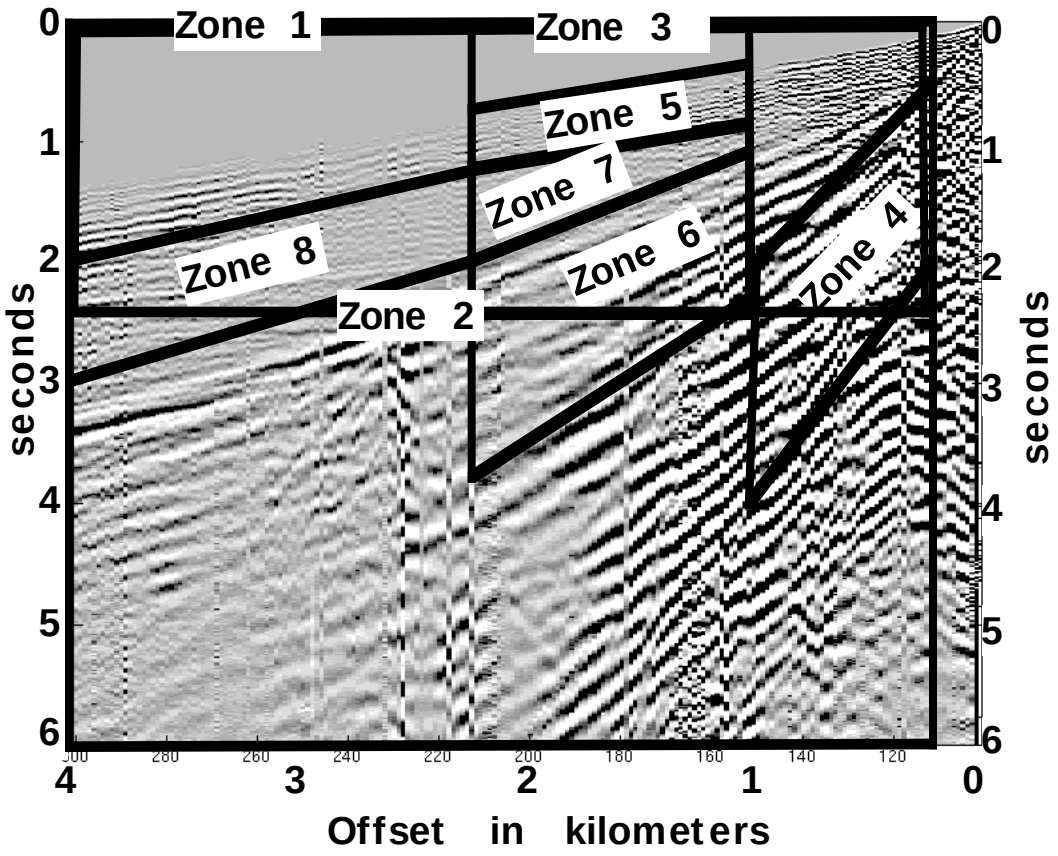

Zone	x1 & x2	times(x1)	times(x2)	comments
1	110 300	0 6	0 6	total record
2	110 300	0 2.5	0 2.5	above basement
3	153 213	0 2.5	0 2.5	above basement 2Hz rec
4	110 150	.4 2	2 4	surface waves
5	153 213	.3 .8	.75 1.25	first breaks
6	153 213	1.1 2.25	2.0 3.75	surface waves
7	153 213	.75 1.1	1.25 2.0	reflections
8	210 300	1.25 2.0	2.0 3.0	reflections

Fig. 40. Shot 101 radial component spectral analysis zones shown on top of 4.5 Hz record..

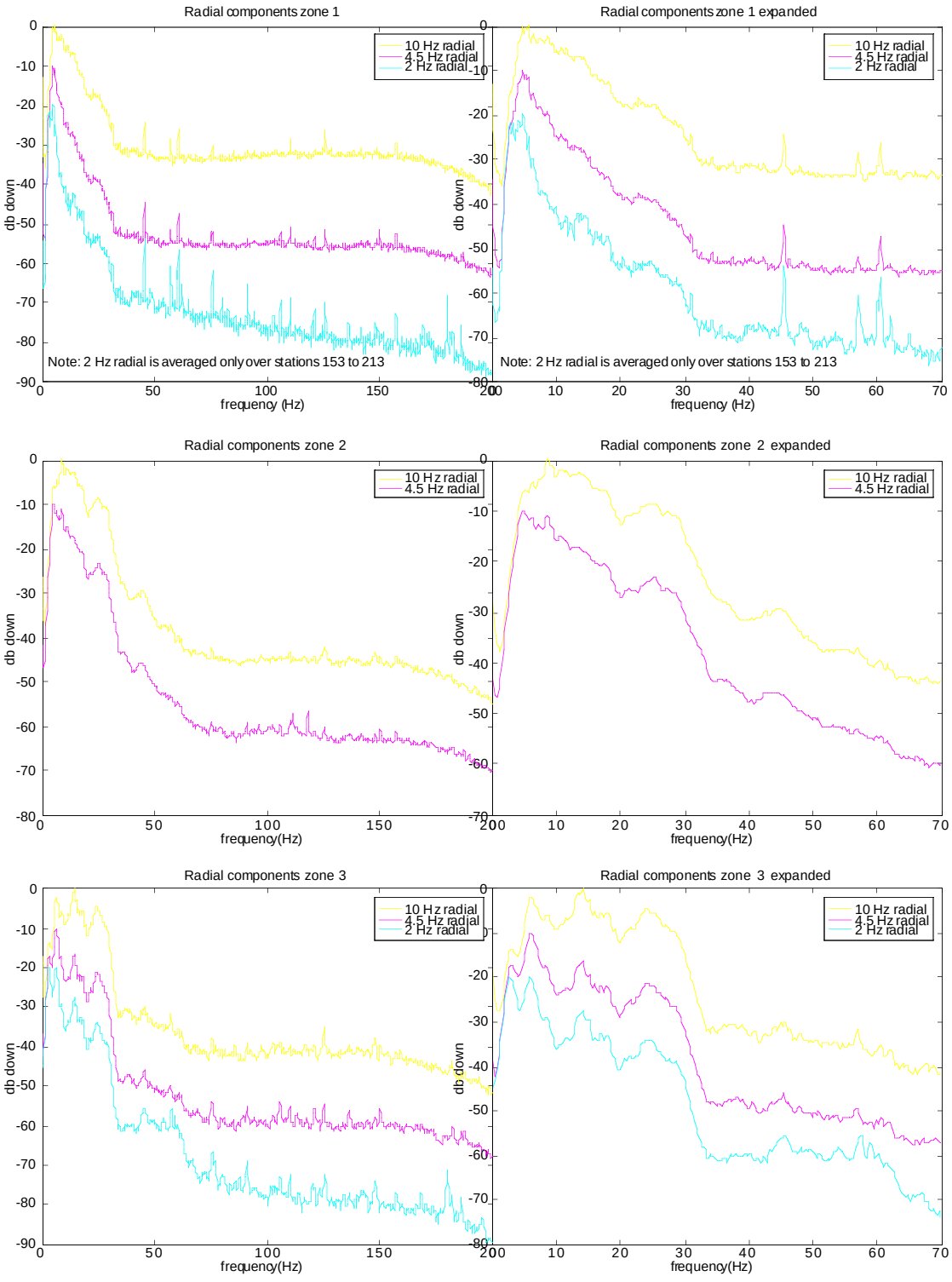

Fig. 41. Averaged amplitude spectra from shot 101 radial component analysis zones 1-3(see fig. 40)

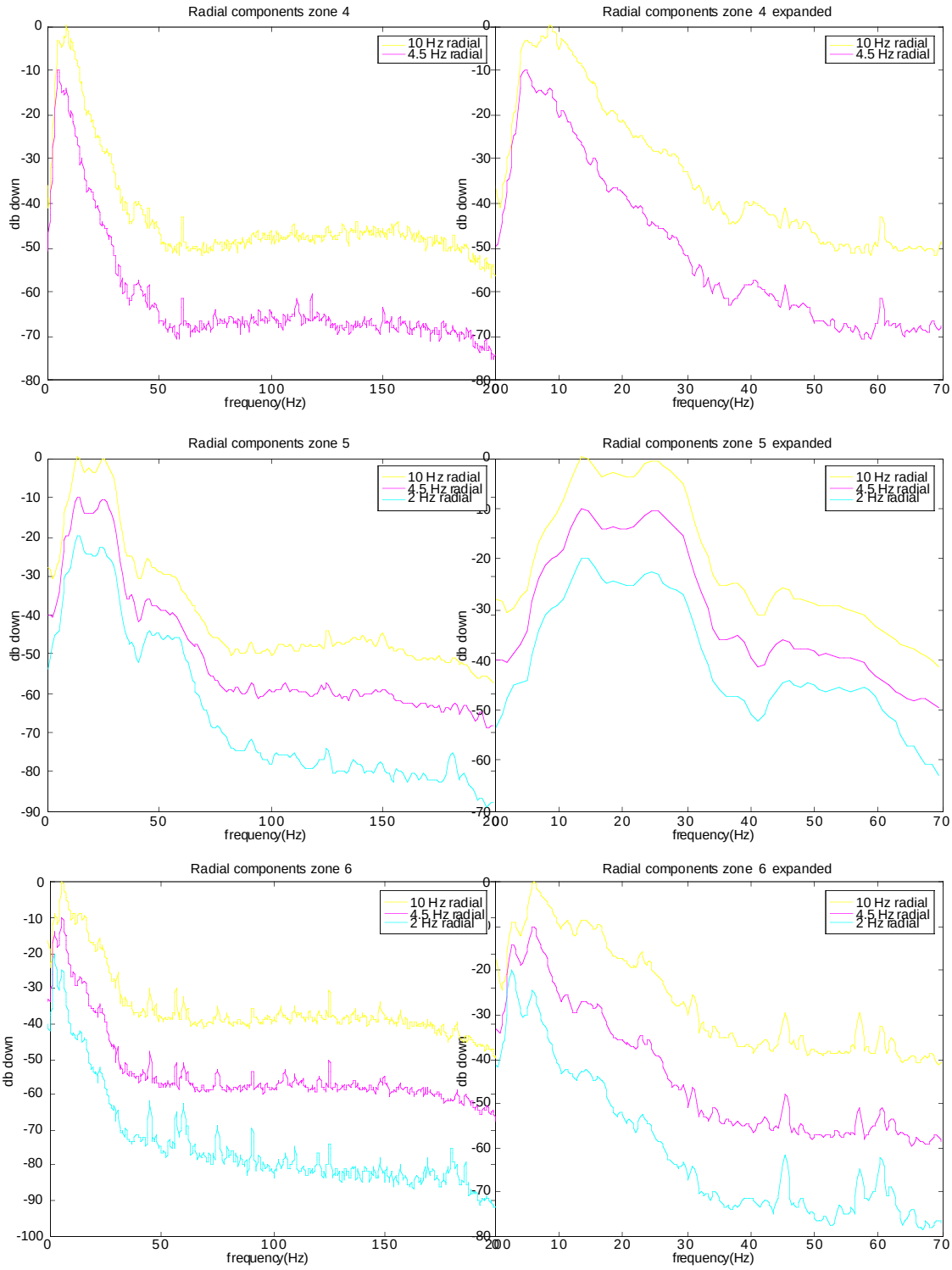

Fig. 42. Averaged amplitude spectra from shot 101 radial component analysis zones 4-6(see fig. 40)

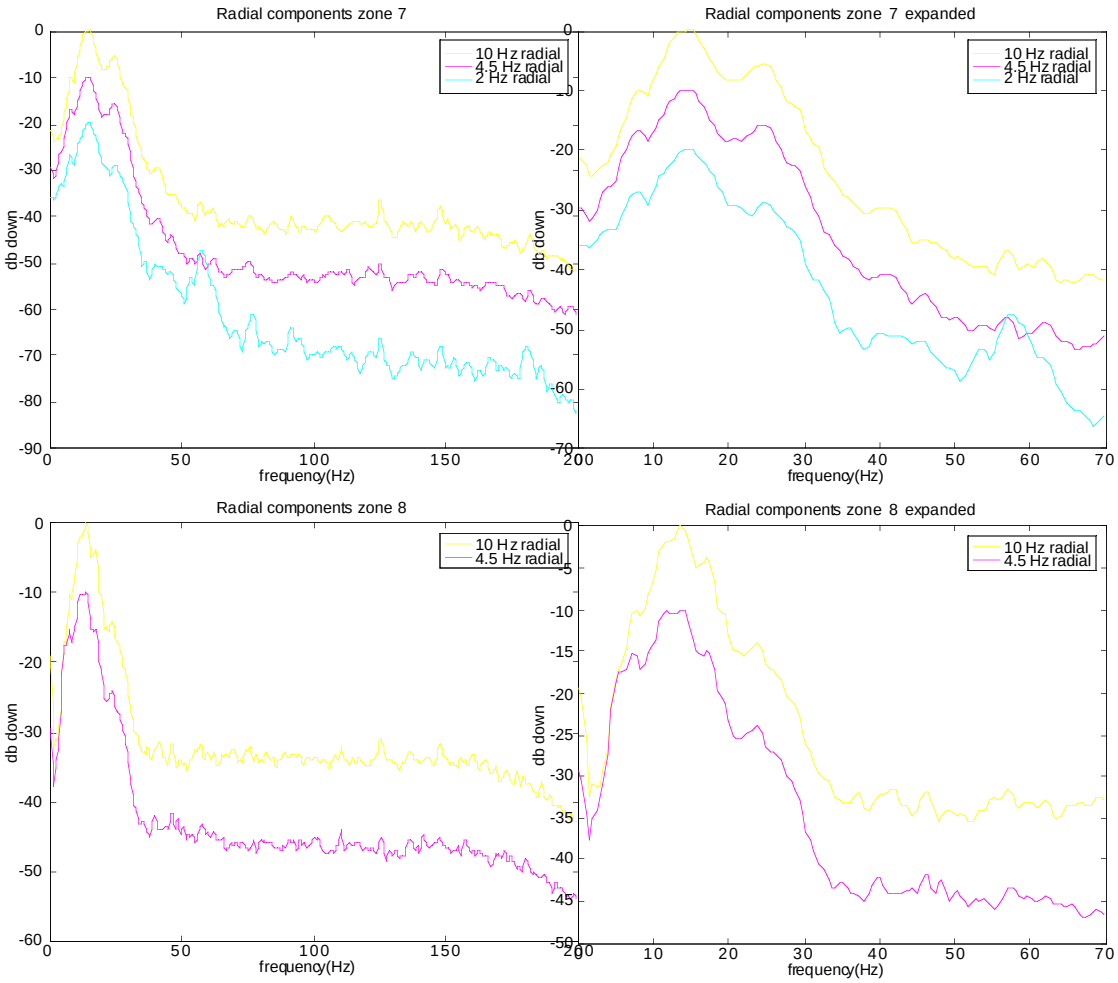

Fig. 43 Averaged amplitude spectra from shot 101 radial component analysis zones 7-8(see fig. 40)